SEDIMENTOLOGY the journal of the International Association of Sedimentologists IAS

Sedimentology (2024) **71**, 116–151 doi: 10.1111/sed.13131

Holocene seismic activity in south-eastern Switzerland: Evidence from the sedimentary record of Lake Silvaplana

BENJAMIN BELLWALD*,†,‡, VALENTIN NIGG§, STEFANO C. FABBRI§, LUKAS W. M. BECKER¶, ADRIAN GILLI‡ and FLAVIO S. ANSELMETTI§

**Norwegian Geotechnical Institute, Sandakerveien 140 NO-0484, Oslo, Norway (E-mail: benjamin.bellwald@ngi.no)*

†Department of Geosciences, University of Oslo, Sem Sælands vei 1 NO-0371, Oslo, Norway

‡Geological Institute, ETH Zurich, Sonneggstrasse 5 CH-8092, Zurich, Switzerland

§Institute of Geological Sciences and Oeschger Centre for Climate Change Research, University of Bern, Baltzerstrasse 1+3 CH-3012, Bern, Switzerland

¶Rambøll Norway, Folke Bernadottes vei 50, Fyllingsdalen NO-5845, Bergen, Norway

Associate Editor – Rick Sarg

ABSTRACT

High-Alpine regions are prone to a large variety of geohazards, among which earthquakes have the strongest impact on landscape and local population. Historic records indicate a moderate to high seismic activity in the northern, south-western and central parts of Switzerland. In contrast, south-eastern Switzerland has less historic earthquake chronicles due to the low population density, resulting in a poorly constrained seismic event catalogue. The aim of this study is to evaluate the palaeoseismic activity for south-eastern Switzerland by using the sedimentary record of Lake Silvaplana in the Engadine Valley. A dense grid of high-resolution two-dimensional seismic profiles, high-resolution bathymetry and a 10 m long sediment core from the deepest basin were used to investigate the stratigraphy of the lake sediments. The bathymetry reveals a flat basin, flanked by steep slopes to the north-west and south-east. The acoustic basement consists of four ridges, and gently-dipping fans to the south-west and north-east. Expressions of slope failure can be identified in all domains of the lake floor and the subsurface data. Multiple coevally-triggered chaotic mass-flow deposits, overlain by megaturbidites with a coarse-sand base, have been detected along ten horizons in the seismic data. The four most recent of these deposits are cored and radiocarbon dated to approximately 230, 310, 960 and 1330 cal yr BP, indicating four over-regional seismic events that triggered large slope failures in Lake Silvaplana in the last 1400 years. Correlation with sediments of Lake Sils, Lake Como, Lake Iseo and Lake Ledro indicate within radiocarbon uncertainties a large earthquake around 1330 cal yr BP. Within their age ranges, the postulated earthquake at 310 cal yr BP (1640 CE) further correlates with a moment magnitude Mw *ca* 5.4 event in Ftan in 1622 CE, and the 960 cal yr BP (990 CE) earthquake correlates with a Mw *ca* 5.2 earthquake in Brescia in 1065 CE. Six mass-movement deposits, also suggested to be caused by earthquakes, were not reached by the sediment core and have suggested ages between 7800 and 11 300 cal yr BP. Thus, Lake Silvaplana sediments provide the first reliable record of seismic activity for the mid and Late Holocene in this region, likely related to the neotectonic activity of the Engadine Line, a major fault zone running along the main valley.

Keywords Alps, deglaciation, earthquake, Engadine Line, geohazards, Holocene, Lake Silvaplana, palaeoseismicity.

INTRODUCTION

Lakes form sensitive and temporally often continuous, high-resolution sedimentary archives that record climatic, environmental, tectonic and anthropogenic changes (Gobet *et al.*, 2003; Gilli *et al.*, 2013; Strasser *et al.*, 2013; van der Bilt *et al.*, 2017). They thus potentially offer archives that can help reconstruct prehistoric natural hazards. Landslides, debris flows, glacier outbursts, storm-triggered floods and snow avalanches are among the best documented natural hazards in the Alps (Huggel *et al.*, 2004; Huss *et al.*, 2007; Badoux *et al.*, 2016). Earthquakes are however an underestimated hazard for lakeshore communities in the Alps, and more palaeoseismic studies are required (Chapron *et al.*, 2016; Kremer *et al.*, 2017, 2020a).

These natural hazards might pose severe risks to infrastructure, dense population centres and tourist destinations. Uncertainties about the intensity and recurrence rates of different types of geohazards complicate decisions for policy makers, potentially resulting in immense economic loss, and, in worst case, loss of lives (L'Heureux *et al.*, 2011; Botzen *et al.*, 2019). The Engadine Valley is a typical inner-Alpine valley, with several hydro-power dams, main traffic roads connecting Switzerland and Italy, and population centres with in total *ca* 25 000 inhabitants hosting *ca* 2 million tourists per year (www.engadin.ch/en), and thus has a high vulnerability to natural hazards (Fig. 1).

Because the limited time span of historical documents does not provide a complete picture of past catastrophic events, the geological archives need to be exploited to reconstruct these events. Previous studies have shown that the most common trigger mechanisms for sublacustrine sediment failures in Alpine lakes are earthquakes, but some of these slope instabilities (i.e. delta failures) may occur spontaneously (Schnellmann *et al.*, 2005; Girardclos *et al.*, 2007; Wirth *et al.*, 2013). Moreover, and adding to the impact of natural hazards, these events are often followed by metre-high tsunami waves originating from the displaced downgoing sediment volumes (Kremer *et al.*, 2014, 2021; Hilbe & Anselmetti, 2015; Nigg *et al.*, 2021). Multiple coevally-triggered mass movements have been used in different subaquatic environments to reconstruct palaeoseismic event catalogues (Moernaut *et al.*, 2007; Strasser & Anselmetti, 2008; Strasser *et al.*, 2013; Bellwald *et al.*, 2016a; Praet *et al.*, 2017). Based on this approach, Kremer *et al.* (2017) compiled a palaeoearthquake catalogue of Switzerland. The Swiss catalogue shows episodes of increased seismic activity at 450, 1600, 2200, 3300, 3900, 6500 and 9700 cal yr BP (Before Present) in central, northern and western Switzerland, with uncertainties of up to 250 years attributed to the earthquake-triggered deposits.

This study conducted a detailed analysis of the sediment fill of Lake Silvaplana to study the Holocene earthquake history of the Engadine Valley with implications on the seismic activity and geohazards of south-eastern Switzerland. Eventually, the study allows expanding the earthquake catalogue of the eastern Swiss Alps and the neighbouring northern Italian area, providing novel insights for the regional seismic and hazard assessment, which is vital to mitigate future disasters.

STUDY SITE

Geological setting

The Upper Engadine Valley, located in south-eastern Switzerland (Fig. 1), is characterized by a complex geology hosting the Austroalpine and Penninic Alpine nappes (Figs 1 and 2). The Austroalpine domain consists of the Margna and Sella nappes in the south, and the Bernina and Err nappes in the north (Fig. 2B; Spillmann & Büchi, 1993). Austroalpine rock types include mostly gabbros, amphibolites, gneisses, green schists and carbonates (Spillmann & Büchi, 1993). The Penninic domain is built up in the area by the Platta nappe, which consists of an ophiolitic sequence originating from the south Penninic realm (Dietrich, 1970).

The Upper Engadine includes four lakes (Sils, Silvaplana, Champfèr and St. Moritz) surrounded by high-Alpine relief with one peak >4000 m above sea level (a.s.l.; Fig. 2A). The valley follows a major geological fault system, the Engadine Line, which is separating the

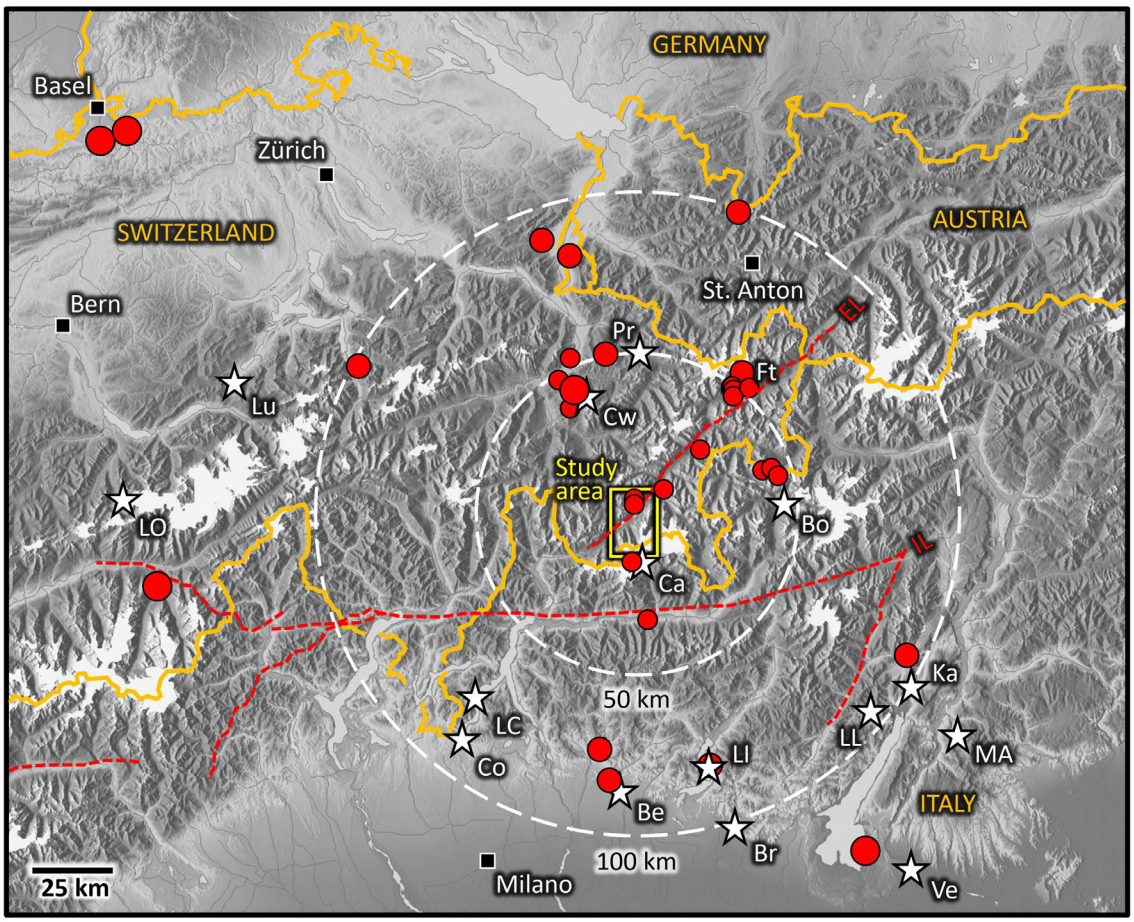

Fig. 1. Seismicity in the study area, located in south-eastern Switzerland, close to the border to Italy and Austria. Shown are all earthquakes with a moment magnitude Mw >6, all earthquakes with a Mw >5 in a radius of 100 km of the study area, and all earthquakes with a Mw >4 in a radius of 50 km of the study area (ECOS-09, 2011; http://map.seismo.ethz.ch/). Indicated as red stippled lines are the two major tectonic lines of the region, the Engadine Line (EL) and the Insubric Line (IL). Other locations mentioned in the text are Be: Bergamo, Bo: Bormio, Br: Brescia, Ca: Chiesa, Cw: Churwalden, Co: Como, Ft: Ftan, Ka: Kas, LC: Lake Como, LI: Lake Iseo, LL: Lake Ledro, LO: Lake Oeschinen, Lu: Lake Lungern, MA: Middle Adige Valley, Pr: Prättigau, and Ve: Verona.

Austroalpine nappes from the Penninic nappes (Fig. 2B). The Engadine Line and the structures of the individual nappes predetermined the drainage system in the Upper Engadine by providing weak, easily erodible zones. The origin of the chain of relatively large glacially-overdeepened lakes in the Engadine Valley is thus both of tectonic and glacial origin, as glaciers tend to follow pre-defined structural weak zones (Schmid & Froitzheim, 1993; Tibaldi & Pasquarè, 2008).

Climate and hydrology

The Engadine Valley is classified as a typical inner-Alpine dry valley (Gensler & Schüepp, 1991). The

Fig. 2. Study area with geological and tectonic information. (A) Catchment of Lake Silvaplana. Hillshade map (SwissAlti3D) modified from Federal Office of Topography swisstopo. x: Location of dated trees located in shallow water depths of Lake Silvaplana and Lake Sils (Schlüchter *et al.*, 2018). ID: Isola Delta. (B) Geological profile crossing the Engadine Valley (modified after Peters, 2005). Emphasis on the different nappes and the Engadine Line. Profile location is shown in (A).

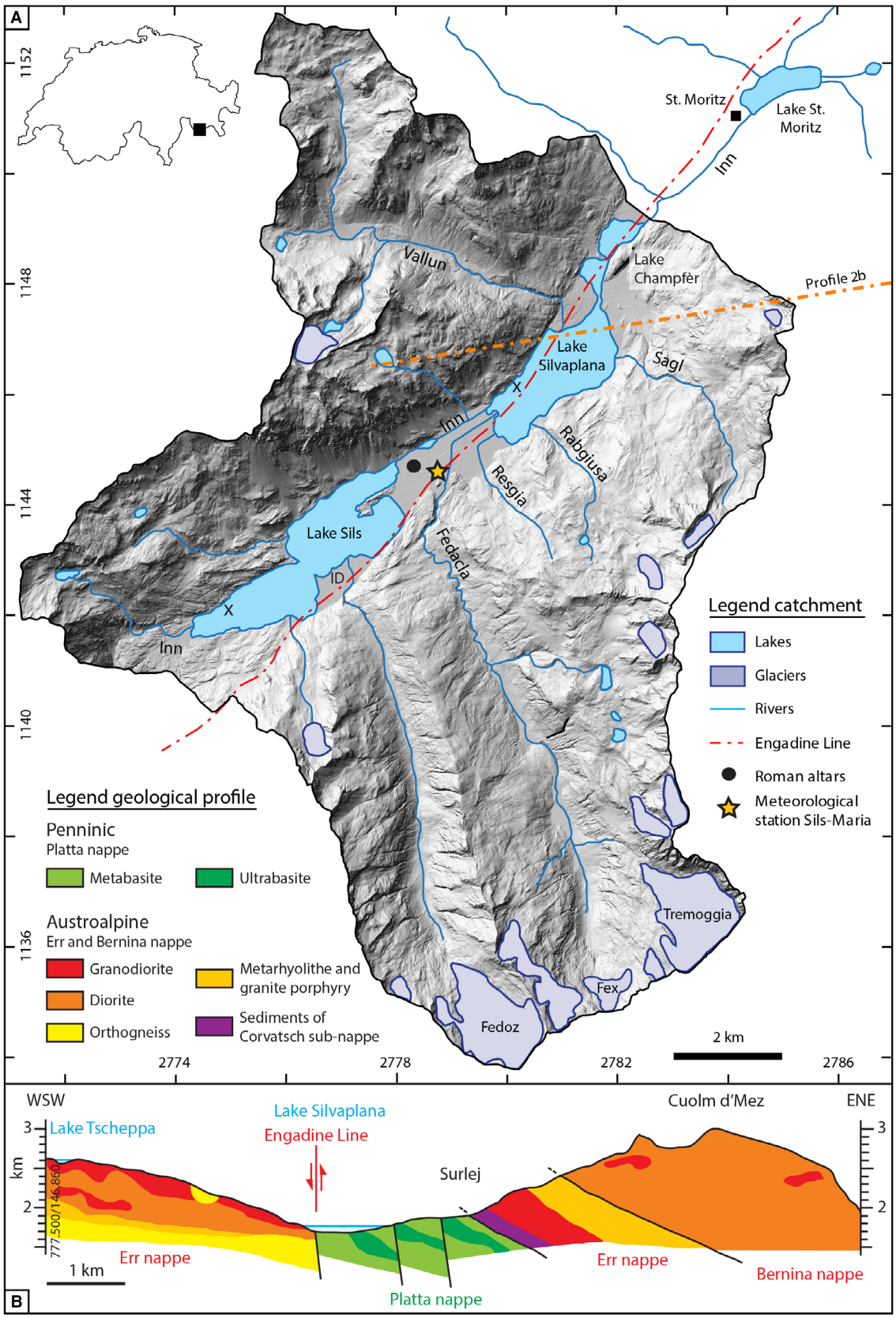

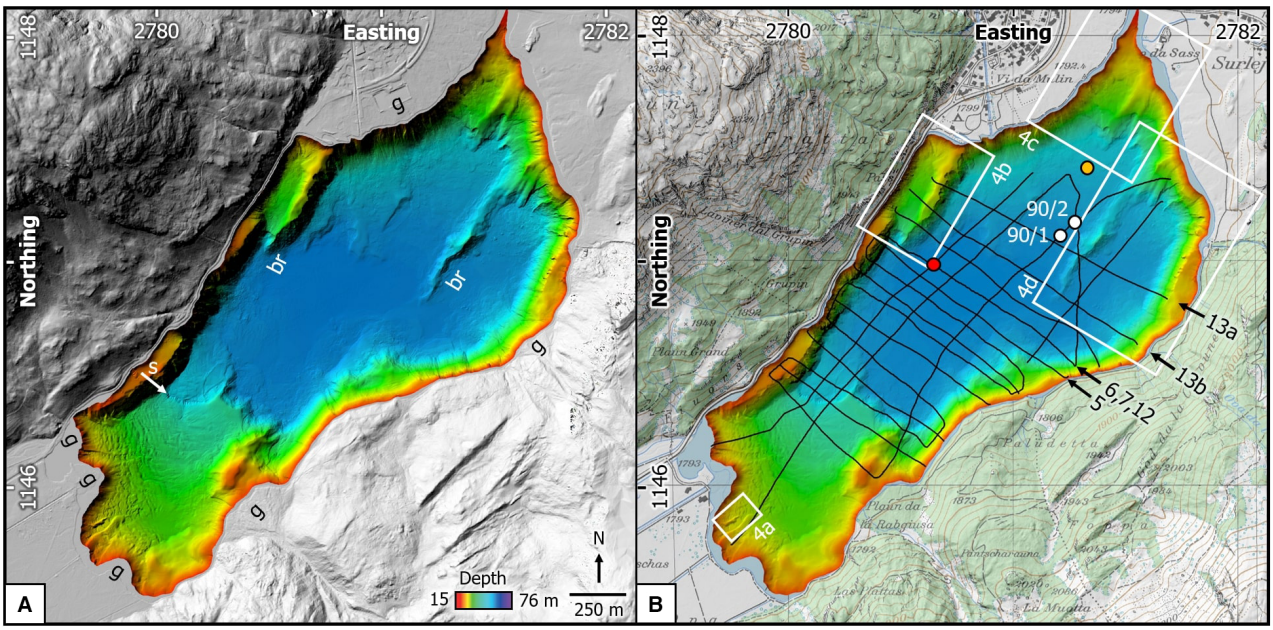

Fig. 3. Bathymetry of Lake Silvaplana. (A) Bathymetry with hillshade relief. White arrow indicates slide scar in deepest basin. (B) Bathymetry with vegetation and blended hillshade relief. Acquired reflection seismic profiles (black lines), seismic profiles shown in this work (black arrows), and long sediment core of this study (SVA12, red dot), as well as cores from previous studies (golden dot for palaeoflood studies, and white dots for piston cores of Leemann & Niessen, 1994) are shown. Topography after Federal Office of Topography swisstopo. g: Gilbert-type delta, br: bedrock ridge, s: slide scar.

annual precipitation at the meteorological station of Sils-Maria (Fig. 2A, 1798 m a.s.l.) is 978 mm with a mean annual temperature of 1.6°C, including seasonal variations between 10.0°C and −7.3°C. Current tree-line, defined by the elevation supporting trees higher than 5 m, lies at 2410 m a.s.l. (Gobet *et al.*, 2003).

Catchment characteristics

Lake Silvaplana is located in the Upper Engadine Valley at an altitude of 1791 m a.s.l., and has an elongated shape with steep lateral slopes (Figs 2A and 3). The lake has a maximum water depth of 77 m, covers 2.7 km^2, comprises a water volume of 127 × 10^6 m^3 and has a water residence time of 0.86 years (LIMNEX, 1994). Maximum seasonal lake-level fluctuations are *ca* 1.9 m (LIMNEX, 1994). The lake freezes over for several months in winter, usually from December/January to April (hydrodaten.admin.ch, null). Rivers are the main sediment contributor to the lake system and drain a partly glacier-covered catchment of 129 km^2 (5% glaciated in 1998; LIMNEX, 2004). The River Inn is the major river connecting all four larger Engadine lakes. Although River Inn has the highest discharge rate into Lake Silvaplana (2.0 m^3 s^{-1}, LIMNEX, 2011), it does not carry much suspended sediment, since suspended particles are mostly deposited in upstream Lake Sils. In terms of sediment load, the most important inflow to Lake Silvaplana is the Fedacla River, characterized by a mean discharge rate of 1.5 m^3 s^{-1} and fed by glacier meltwater from the Tremoggia and Fex glaciers. The River Vallun (0.7 m^3 s^{-1}) and River Sagl (0.3 m^3 s^{-1}) are further important inflows (LIMNEX, 1994). Historical lacustrine records show that intensive snow melt as well as intense and long-lasting precipitation events with high mass-accumulation rates repeatedly occurred in the Upper Engadine (Ohlendorf *et al.*, 1997; Blass *et al.*, 2005, 2007a, b; Caviezel, 2007; Trachsel *et al.*, 2008). Flood records of previous studies in Lake Silvaplana are limited to 3000 to 1500 cal yr BP (Stewart *et al.*, 2011a) and the last 850 years (Trachsel *et al.*, 2010).

Lake-infill history

The glaciers in the study area were most extensive between 30 ka and 18 ka and retreated behind Lake Silvaplana after the Younger Dryas (*ca* 14.6 ka; Ivy-Ochs *et al.*, 2008; Ilyashuk *et al.*, 2009). The summit of the Inn glacier system was located above St. Moritz and Samedan at a maximum of 2900 m a.s.l. and probably at *ca* 2800 m a.s.l. during the Würm Glacial (last glacial period, Maisch, 1992). After a reduction in ice thickness during the Late Glacial, the glacier floated up so that sediments could accumulate at the ice base in a subglacial lake (Schlüchter, 1987).

Inflowing rivers delivering the clastic particles erode Penninic and Austroalpine rocks and drain a catchment of 129 km^2 (Fig. 2A). Clastic sedimentation is dominant in Lake Silvaplana, but autochthonous production increased due to recent eutrophication (Ohlendorf *et al.*, 1997). Annually laminated sediments (varves) were continuously deposited in Lake Silvaplana for the last 3300 years, combined with sedimentation rates up to nine times higher than in the interval from 8000 to 5000 cal yr BP (Leemann & Niessen, 1994). Varves are not detected in neighbouring Lake Sils, making Lake Silvaplana the preferred place to study palaeofloods and palaeoclimate (Leemann & Niessen, 1994; Blass *et al.*, 2007a,b; Trachsel *et al.*, 2008). Eighty-five palaeoflood layers have been identified from turbidites in sediments of Lake Silvaplana (Stewart *et al.*, 2011a). These turbidites show a higher frequency during cool and/or wet phases of *ca* 1450 Before Common Era (BCE, 3400 cal yr BP) to 420 Common Era (CE; 1530 cal yr BP; Stewart *et al.*, 2011a).

The presence of glaciers within lake catchments affects lacustrine sedimentation. During periods of glacial readvances and retreats, lacustrine sedimentation is dominated by increased riverine input of silt-sized and clay-sized material delivered by glacial meltwater (Leemann & Niessen, 1994). Rates of erosion are generally higher for glacial than for non-glacial catchments (Church & Slaymaker, 1989; Bogen, 1996; Glur *et al.*, 2015).

Pollen assemblages from sediment cores of downstream Lake St. Moritz and Lake Champfèr show human impact in the Upper Engadine from around 5500 cal yr BP onward. Marked vegetation changes and regular cereal cultivation started *ca* 3900 cal yr BP (Gobet *et al.*, 2003). Evidence for regional deforestation was found in pollen and charcoal data from sediment records of Lake St. Moritz between 700 and 1700 CE (Gobet *et al.*, 2003).

Palaeoseismicity

The Swiss earthquake catalogue documents strong prehistoric and historic earthquakes (Mw >6) to have occurred within the study area (Fig. 1; ECOS-09, 2011). In Churwalden, located *ca* 35 km north-west of the Engadine Line, the most significant earthquake was documented in 1295 CE, characterized by a moment magnitude of Mw 6.5 ± 0.5 and an assessed epicentral intensity of VIII (Schwarz-Zanetti *et al.*, 2004). In Ftan, *ca* 50 km to the east of Lake Silvaplana, a Mw 5.4 earthquake hit the region in 1622 CE (ECOS-09, 2011). More recently, in December 1999, a Mw 4.9 earthquake occurred in Bormio (ECOS-09, 2011), located *ca* 40 km to the east of the Engadine Line. In the last 1000 years, the region around Lake Silvaplana (radius of 50 km) was hit by 17 earthquakes with moment magnitudes of Mw >4, epicentral intensities of V to VIII, and focal depths of 5 to 15 km (ECOS-09, 2011). Although these palaeoearthquakes could not yet be related to the Engadine Line, the fault system of the Engadine Line is considered to be a seismically active structure with low-magnitude historical events (Albini *et al.*, 1988). Prehistoric earthquakes likely have contributed to the triggering of deep-seated gravitational slope deformations (Tibaldi & Pasquarè, 2008).

In upstream Lake Sils, an up to 6 m thick megaturbidite, originating from a partial Isola Delta collapse with a depositional volume of 6.4×10^6 m^3, has been radiocarbon dated to 550 to 800 CE (Fig. 2; Blass *et al.*, 2005). Onshore and in the shallow environment of Lake Sils, a peat layer is overlain by a centimetre to decimetre thick layer consisting of gravelly sand to fine silt (Nigg *et al.*, 2021). Moreover, within this clastic layer, Roman altars have been found in 1964 CE (Erb *et al.*, 1966). Nigg *et al.* (2021) suggested that this layer represents a palaeotsunami deposit ultimately caused by waves triggered by the above-described delta collapse. An undocumented earthquake dated to the 6th century is suggested as a trigger mechanism for deformations in a stratigraphic sequence and an archaeological site in Como city (Livio *et al.*, 2023). Additionally, two megaturbidites in Lake Como at a distance of 90 km have been suggested to be caused by seismic shaking in the 6th and 12th

centuries (Fanetti *et al.*, 2008). The thickest large-scale mass wasting deposit of Lake Iseo, 85 km to the south of Lake Silvaplana, is dated to 1191 ± 62 CE (Lauterbach *et al.*, 2012). In a more recent study of that lake, the three thickest mass movements have been suggested to be triggered by earthquakes in 1222 CE, 1117 CE and 700 CE (Rapuc *et al.*, 2022).

DATA AND METHODS

Bathymetric data

High-resolution bathymetric data have been acquired in October 2019 using a Kongsberg EM2040 multibeam echosounder (Kongsberg Gruppen ASA, Kongsberg, Norway) in 1° by 1° beam–width configuration. The device operates at 300 kHz and records 400 depth detections per pulse, with a ping rate of up to 20 Hz in shallow waters. A Leica GX1230 GNSS receiver (Leica, Wetzlar, Germany) was used for positioning in combination with the swipos-GIS/GEO real time kinematic positioning system provided by swisstopo. The survey lines were carried out in a shore-parallel pattern to guarantee best detection quality along steep shorelines. Key processing steps involved the merging of all auxiliary-sensor data (motion sensor, heading sensor, sound velocity sensor, positioning), and reviewing and manually correcting them if erroneous recordings occurred. A gridded dataset with a 1 m cell size and a vertical resolution of a few centimetres in shallow water (<30 m depth) to decimetres (deeper basin, >60 m depth) was produced for morphological analysis (Fig. 3).

Seismic data

High-resolution reflection seismic profiling was conducted with a 3.5 kHz single-channel pinger system (Geoacoustics Limited, Great Yarmouth, UK) containing four piezoelectric transducers during two field campaigns in 2005 and 2011. Approximately 20 km of 2D seismic data were collected with a cruise speed of 5 km h^{-1} and a shooting interval of 0.5 s (Fig. 3B). Positioning data were obtained by a GPS system mounted directly on the sender/receiver assembly, resulting in an accuracy of ±5 m. The seismic signal reached a maximum penetration of 75 m (100 ms TWT) with a vertical resolution of *ca* 10 cm. The seismic profiles have later been interpreted using the software Kingdom™. Two-way-travel times (TWT) were converted into more comprehensible depths below lake surface assuming conventional P-wave velocities of 1450 m s^{-1} for water and 1500 m s^{-1} for sediment. A quasi-3D seismic analysis of the sedimentary fill of the basin was obtained from the seismo-stratigraphic interpretation. This detailed analysis was the base to select ideal coring sites, define sediment packages, and establish a seismo-stratigraphic framework. Four seismic facies were defined, which have been distinguished by criteria such as continuity, reflection amplitude and depositional geometry. The upper and lower boundaries of the different turbidites, megaturbidites and associated slide wedges were interpreted in the seismic data of the entire basin. The volumes of the megaturbidites were estimated by gridding these boundaries in the SURFER8® software. In addition, the sediment cores of former studies were localized on the seismic grid to calibrate the lake stratigraphy (Fig. 3B).

Sediment-core analysis

Two 10.5 m long piston cores were recovered from the frozen lake surface in March 2012 using a UWITEC percussion piston-coring system (UWITEC, Mondsee, Austria; SVA12-2 and SVA12-3, position in Swiss Grid LV95: 2780640/1146976; same location for both cores). The cores were retrieved in the deepest part of the basin at 76.4 m water depth within an area of relatively well-stratified sediments intercalated by one large mass-movement deposit that is overlain by a thick, acoustically transparent body with a smooth surface. Minimal hiatuses along the core were guaranteed by selecting a coring site where sedimentary deposits in the seismic profiles showed a low degree of erosive behaviour. The long core was retrieved in 3 m long sections, which were subsequently cut into three smaller parts (*ca* 1 m in length). The first long core (SVA12-2) has sections from 0 to 3 m, 3 to 6 m and 6 to 9 m subsurface depth, whereas the second long core (SVA12-3) reaches from 1.5 to 4.5 m, 4.5 to 7.5 m and 7.5 to 10.5 m subsurface depth (Fig. S1). Using a hammering short-coring device, a short sediment core (SVA12-1) was collected from the same site to calibrate the long cores by obtaining the undisturbed sediment–water interface. A composite section has been established from the cores taken with slight lateral offset and an overlap of 150 cm (Fig. S1) through a macroscopic layer-to-layer correlation.

Petrophysical sediment analysis was conducted on the unsplit core sections using a GEOTEK multi-sensor core logger (Geotek Limited, Daventry, UK), and allowed measuring wet-bulk density, magnetic susceptibility and P-wave velocity throughout the core at intervals of 0.5 cm for 10 s. The P-wave velocities obtained from the GEOTEK measurements of the sediment cores are not continuous so that they were not used to convert time to depth. After the core segments were split lengthwise, core photographs were taken immediately to avoid changes related to oxidation and drying. The single photographs of the 20 cm long core intervals were merged. After photography, a sedimentological description was done and samples of selected intervals were sieved for grain-size analysis. Grain size, organic matter, mica and vivianite of the event layers were analysed visually. Using all of the described results, a classification consisting of four lithotypes was established.

Chronology

The cumulated thickness of event layers (turbidites and mass flows) was subtracted and a background sediment column (event-free sediment depth) was generated to obtain a solid chronology and background sedimentation rates. The thickness of the background sediment section measures *ca* 6 m. To date the past mass movements, the top of each turbidite deposit was determined and a specific stratigraphic horizon was created for every event (Table S1). These stratigraphic horizons are acting as timelines. Precise core-to-seismic correlation allowed to date the event horizons defined in the seismic profiles, and to establish distribution and volumes of mass movements.

Eight samples were taken within hemipelagic sediments for radiocarbon dating from the long sediment core. The material was a piece of wood for one sample and larches (Larix) needles sieved from 0.5 cm intervals for the other seven samples (Table 1). Samples were radiocarbon-dated at ETH Zurich and at the Laboratory for the Analysis of Radiocarbon with AMS (LARA) of the University of Bern (Table 1; Szidat *et al.*, 2014). Obtained radiocarbon ages were calibrated using OxCal (version 4.4; Ramsey, 2009) and the IntCal13 calibration curve (Reimer *et al.*, 2013). Additionally, the uppermost 30 cm of the short sediment core were sampled in 0.5 cm intervals and measured with a gammaspectroscope for ^{137}Cs radionuclides. The age model for the background sedimentation in the core is based on these two tie points (1963 and 1986) as seen in the ^{137}Cs peaks (Appleby, 2001; Cohen, 2003), combined with the eight AMS radiocarbon (^{14}C) dates. The uppermost point of the age model represents the year 2012, the year the sediment core was

Table 1. Calibrated radiocarbon ages from terrestrial organic macro-remains used for the age-depth-modelling.

Sample code	Core ID	Composite depth (cm)	Background depth (cm)	Sample description	Sample material	^{14}C age ± 1σ (^{14}C years BP)	Calibrated 1σ (cal ^{14}C years BP)	±1 s (cal. yr)	Probability (%)
BE-12175.1.1	SVA12-2-1B-31	110	65.5	Needle fragments	Macrofossil	193 ± 83	165.5	165.5	87.0
BE-12176.1.1	SVA12-3-1B-58	290	233.0	Needle fragments	Macrofossil	996 ± 74	899.5	158.5	95.4
BE-12180.1.1	SVA12-3-1C-09	345	270.0	Needle fragments + birch seed	Macrofossil	1275 ± 69	1180.0	125.0	94.5
ETH-46611	SVA 12-2-2A-03	399	303.5	Wood	Wood	1445 ± 25	1340.0	40.0	95.4
BE-12181.1.1	SVA12-2-3B-29	660	361.0	Needle fragments	Macrofossil	2027 ± 52	2000.0	123.0	95.4
BE-12177.1.1	SVA12-3-3A-24	740	430.5	Needle fragments	Macrofossil	2604 ± 77	2655.0	220.0	95.4
BE-12178.1.1	SVA12-3-3B-33	850	520.5	Needle fragments	Macrofossil	3106 ± 32	3308.5	78.5	95.4
BE-12179.1.1	SVA12-3-3C-98	1000	624.5	Needle fragments	Macrofossil	6791 ± 63	7660.5	98.5	93.2

collected. The radiocarbon dates were calibrated within the Bayesian age modelling package 'rbacon' (v2.3.6) in R (Blaauw & Christen, 2011). Ages are given in cal yr BP, where BP is the year 1950.

Discrimination between seismically-triggered and flood-triggered deposits

Multiple mass-flow deposits and associated overlying megaturbidites (>10 cm thick) along a single stratigraphical horizon in seismic data are key criteria to identify a seismic trigger mechanism (Schnellmann *et al.*, 2002, 2006; Strasser *et al.*, 2006; Strasser & Anselmetti, 2008; Bellwald *et al.*, 2016a, 2019a; Kremer *et al.*, 2017). Small-scale mass-movement event deposits, however, cannot be resolved by the seismic data, in particular on the delta slopes characterized by a lower signal penetration and lower signal quality. Sediments accumulated on the deltas can fail and produce a turbidite without requiring an external trigger, but mass-flow deposits from lateral slopes lacking any major riverine input are required to define a seismically-triggered event (Strupler *et al.*, 2018).

Turbidites lacking any association with slide wedges and deformed sediments, that were generally thinner (<10 cm) but with stronger magnetic susceptibility excursions, were interpreted as flood events. In contrast, mass-flows originating from lateral flanks of the lake are supposed to produce thicker turbidites in the deepest part of the basin of Lake Silvaplana, from where the sediment core is taken. However, our study cannot differentiate beds deposited by flood events from small-scale delta collapses that remobilize former flood material. Consequently, the 53 thinner turbidites (<10 cm) were all interpreted as flood-related deposits.

Following the definition of Baker (2008) for natural hazards, palaeoearthquakes were defined as ancient earthquakes that occurred without being recorded by either direct seismic measurement or observed by any seismologist. The palaeoseismic events postulated in this study are compared to existing historic and prehistoric earthquake catalogues, the latter derived from mass-movement deposits in surrounding lakes (Lake Como, Lake Sils), a Swiss compilation (Kremer *et al.*, 2017, 2020a) and studies representative for palaeoseismic activity in northern Italy (Lauterbach *et al.*, 2012; Simonneau *et al.*, 2013; Rapuc *et al.*, 2022). The earthquakes listed in the inventory of the Swiss Seismological Service were also included (ECOS-09, 2011; seismo.ethz.ch; Fig. 1).

RESULTS

Bathymetry

The deepest point in Lake Silvaplana is at 77 m water depth with respect to an 89 year long (1928 to 2017) average lake level of 1790.5 m a.s.l. (datum LN02) based on the gauging station Silvaplanersee (LH2073, BAFU). The bathymetry of Lake Silvaplana is characterized by a flat lake basin flanked by steep slopes in the north-west and south-east, mirroring the morphology of the Upper Engadine Valley axis (Fig. 3). Gently-dipping slopes are identified to the north-east and south-west of the lake, where the largest rivers enter the lake (Fig. 4A to C). These areas are characterized by sub-lacustrine convex-shaped fans, which are interpreted as Gilbert-type fluvial deltas ('g' on Fig. 3A). Two elongated sharp ridges cross the lake in a north-east/south-west direction ('br' on Figs 3, 4B and 4D). A prominent step is identified in the south-west of the flat basin ('s' on Fig. 3), crossing the basin in a north-west/south-east direction.

A large variety of expressions indicating slope failure are identified along the lake floor, which include: (i) cyclic steps on the Resgia, Fedacla and Inn Delta in the west of the lake (Fig. 4A; Clarke *et al.*, 2014; Bellwald *et al.*, 2016b; Slootman & Cartigny, 2020); (ii) small amphitheatre-shaped headwalls along the steep flanks of the ridges and along the steep flanks in the north-west of the lake with lobe deposits onlapping the slope flanks and remobilized blocks further downslope (Fig. 4B to D); (iii) linear gullies in the north of the lake (Fig. 4C); and (iv) large amphitheatre-shaped headwalls in the basin of the lake ('s' on Fig. 3).

Seismic facies analysis

The seismic lines generally show a good penetration of the acoustic signal down to a maximum sub-surface depth of *ca* 100 ms TWT (*ca* 75 m; Figs 5 to 7). Penetration is highest in the deepest basin (Fig. 8). However, within the deltaic environments, the seismic penetration is reduced to <10 m. Four seismic facies (SF) were identified in the stratigraphy of Lake Silvaplana (Table 2; Figs 5 and 6). Continuous reflections of moderate amplitude which are draping the

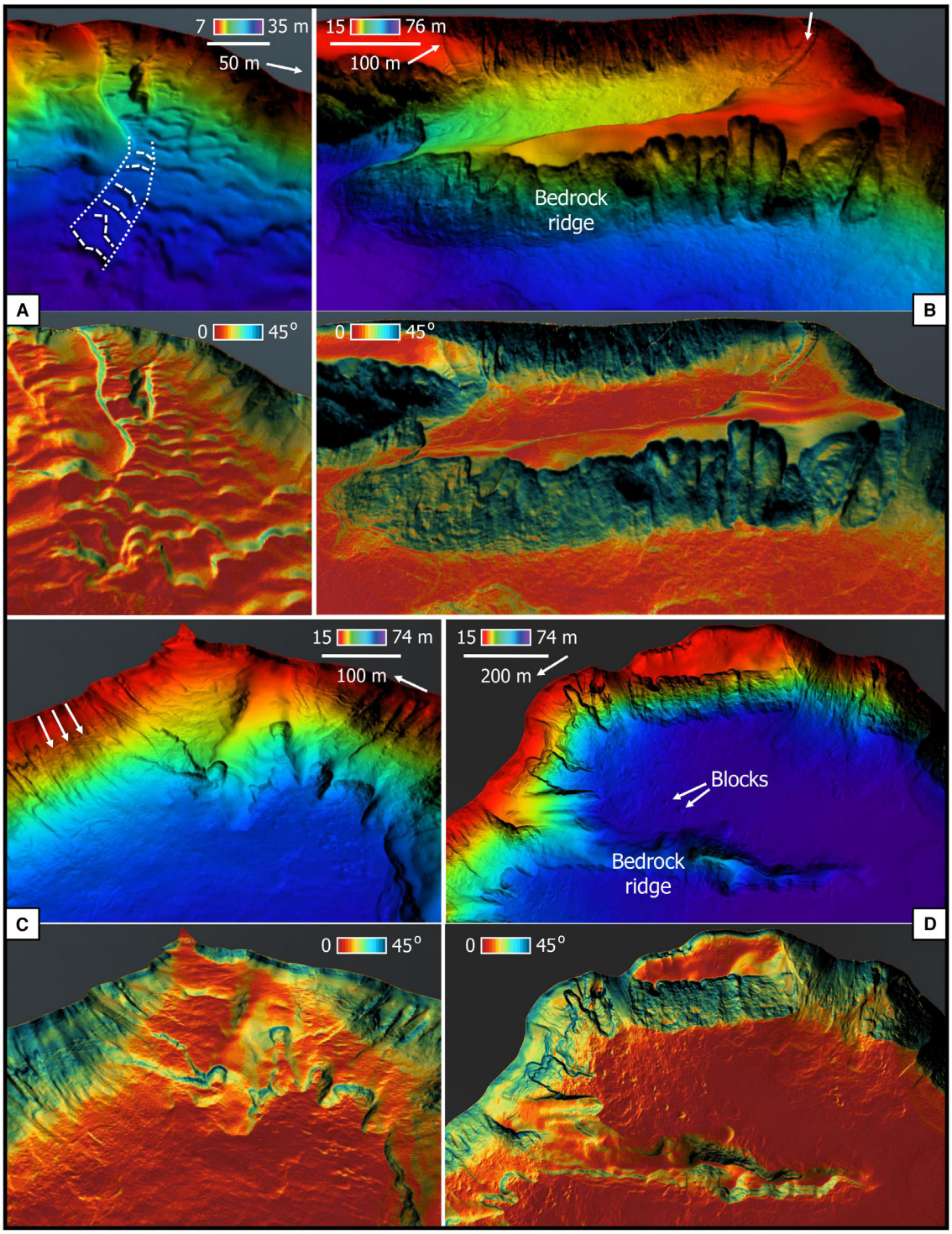

Fig. 4. Selected highlights of bathymetric dataset, shown both in depth and slope gradient. (A) Cyclic steps shaping the Resgia, Fedacla and Inn Delta. (B) Bedrock ridge with amphitheatre-shaped escarpments. Channel from the Vallun River is indicated by white arrow. (C) Deeply carved escarpments of the Vallun Delta. Linear gully-type slope failure characterizing the Vallun Delta is shown by white arrows. (D) Slope failures along steep lake flanks. Slide blocks and bedrock ridge are indicated. For figure location, see Fig. 3B.

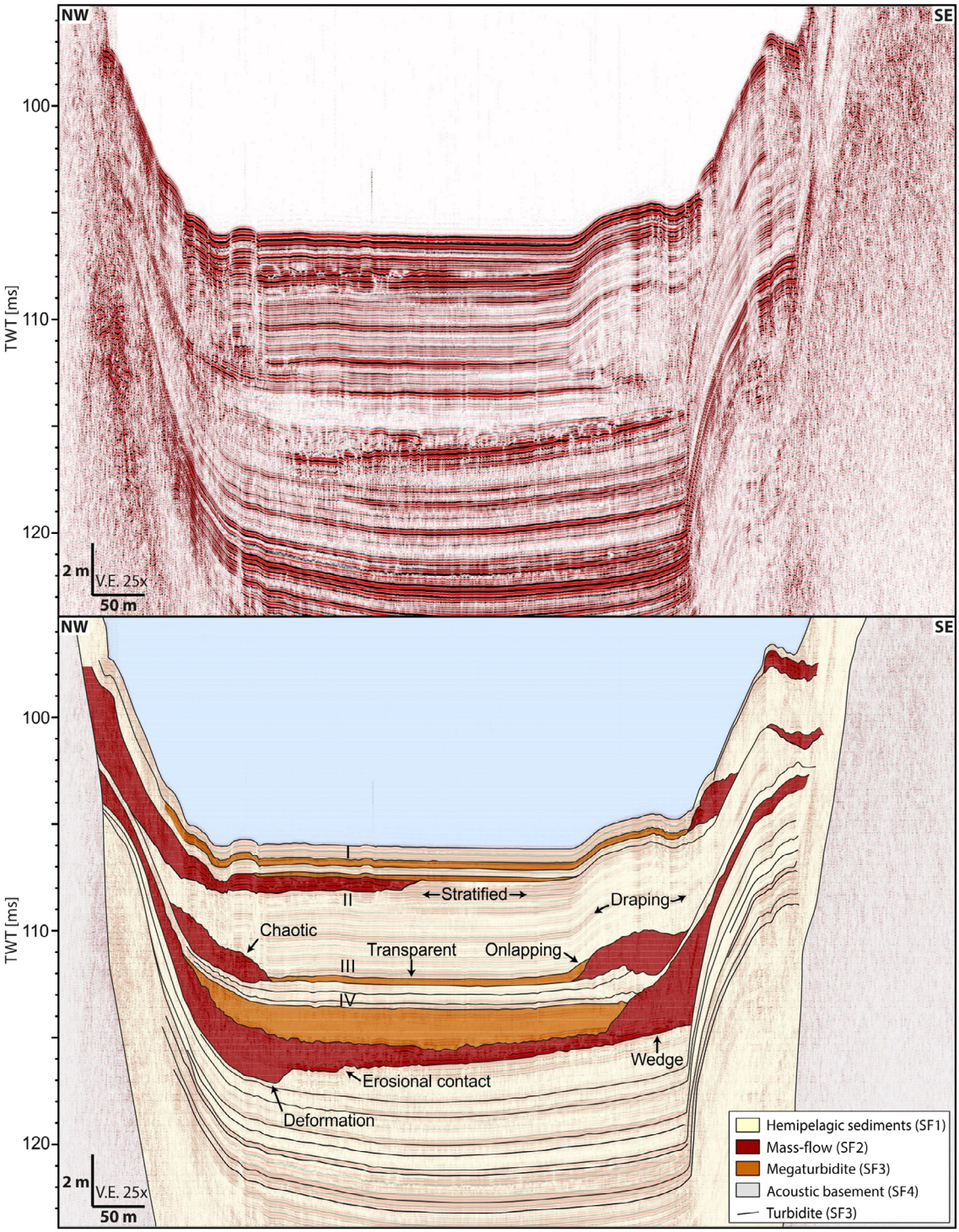

Fig. 5. Seismic profile across the central basin displaying variable seismic facies (SF): SF2 and SF3 are interpreted as mass-movement deposits. Note the difference in ponding and onlapping behaviour of SF3 compared to the well-stratified and draping layers defining SF1. The profile shows the uppermost four palaeoseismic events (SF2 and SF3, indicated as I–IV) and flood events detectable in the reflection seismic data (black lines). For profile location, see Fig. 3B.

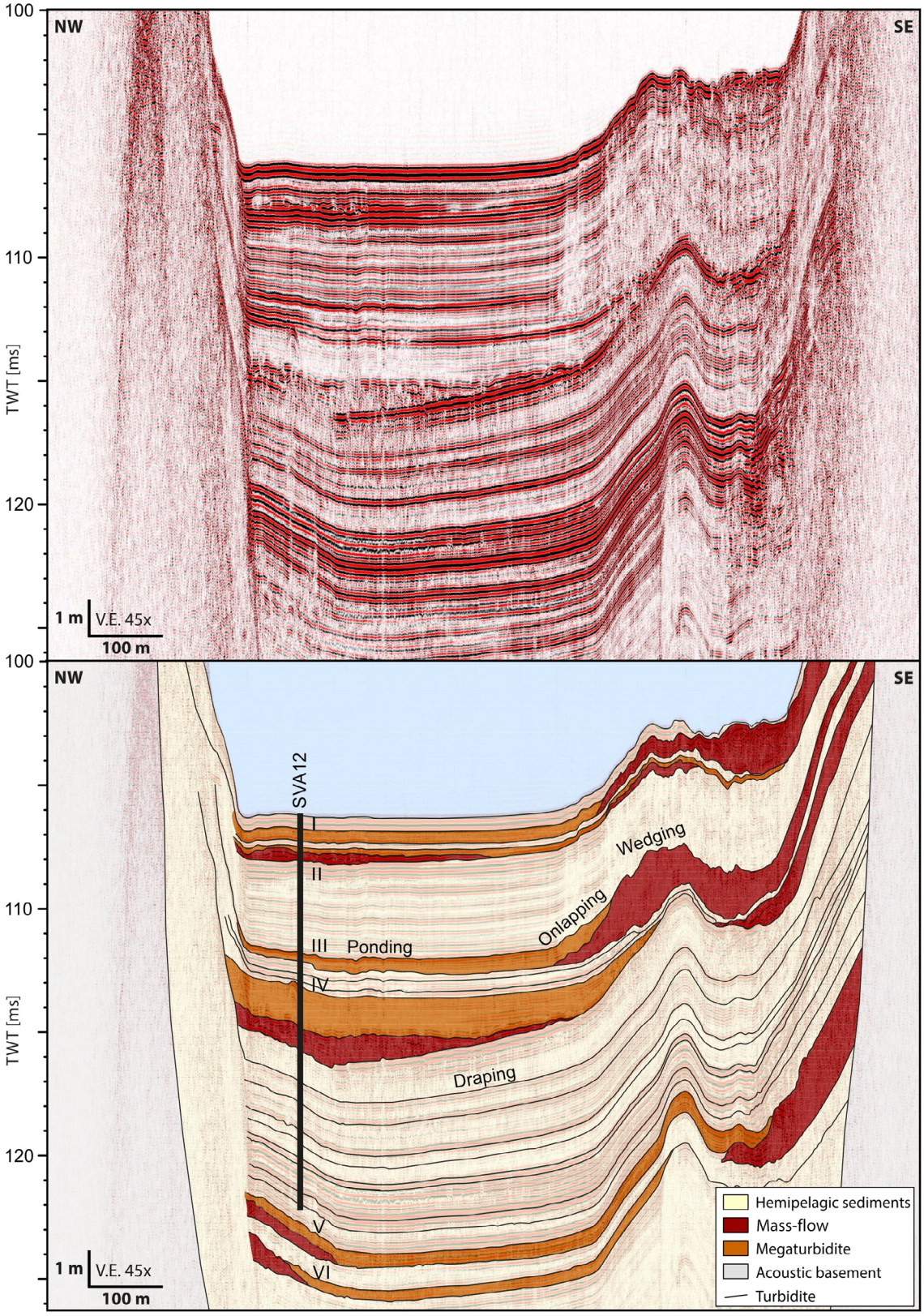

Fig. 6. Seismic profile across Lake Silvaplana with coring site for long sediment core SVA12 (black bar). The core penetrates the deposits of four earthquake-triggered megaturbidities (indicated as I–IV; V and VI have not been penetrated). Flood events detectable in seismic profiles are shown as black lines. For profile location, see Fig. 3B.

pre-existing topography characterize SF1. This facies can be identified throughout the lake infill. SF2 is defined by chaotic reflections of moderate to high amplitudes with irregular sharp boundaries and erosive basal contacts. The upper boundary can have a bulging character. The facies has a wedging character in profile view, and builds lobes with radial decrease in thickness in planar view. Several of these wedges have been recognized along ten different continuous seismic reflections (Fig. 7). This facies mainly occurs along the lake flanks and the ridges. SF3 consists of transparent units of low amplitudes bounded by reflections of high amplitudes both to the top and bottom. The reflections defining SF3 are onlapping the wedges of SF2. The volumes defined by the top and base reflection of SF3 vary from 25 000 to 292 000 m^3. SF3 is exclusively deposited in the deepest part of the basin. The sediments characterizing this facies are deposited within one depocentre for eight deposits, and two depocentres have been mapped for two deposits. While SF1 to SF3 have been cored, a fourth seismic facies (SF4) was identified that could not be reached by coring (Figs 6 and 7). This facies is characterized by scattered internal reflections, and forms two large north-east/south-west oriented ridges at the lake floor, with an elevation of about 25 ms (or *ca* 19 m) compared to the surrounding lake floor ('br' on Fig. 8). Two north-west/south-east oriented ridges of SF4 cross the lake, but are not expressed at the lake floor ('mr' on Fig. 8). However, one of these ridges correlates with the large headwall in the flat basin.

Sedimentology

Based on the results of the detailed core analysis (Fig. 9), four lithofacies (LF1 to LF4) were defined (Fig. 10; Table 2). LF1 comprises all laminated lithologies. They have been interpreted in previous studies as mostly varves (Leemann & Niessen, 1994; Blass *et al.*, 2007a,b; Trachsel *et al.*, 2008, 2010; Stewart *et al.*, 2011b). Two subtypes of laminated lithofacies were distinguished: LF1a is characterized by silty to clayey laminations with densities from 1.2 to 1.6 g cm^{-3} and magnetic susceptibilities of 20 to 30 × 10^5 SI. The laminations of LF1a are bright and <0.5 cm thick (Fig. 10A), and occur in the uppermost 8.5 m of the core. The thicker laminae of LF1a have a coarser grain size and are highly variable in colour (light grey, dark grey, light brown), whereas the thinner laminae of LF1a are fine-grained and different in colour (orange-brown, brown, greenish-brown). A second type of lamination (LF1b) is dark, more sticky, low in water content, contains gas cracks and is <1 cm thick. The laminations of LF1b are thicker and darker than those described in the bright lamination lithotype defining LF1a (Fig. 10B). The darker laminations (LF1b) dominate the lowermost 1.5 m of the sediment core (Fig. 9). Deformed silty to clayey sequences with a patchy, mottled pattern define LF2 (Fig. 10C). The lithofacies occurs in packages thicker than 10 cm with densities of 1.4 g cm^{-3} and magnetic susceptibilities of 20 to 30 × 10^5 SI. LF3 is characterized by normal grading from coarse sand to fine clay overlain by homogenous clay with few sandy intercalated layers towards the base (Fig. 10D and E). The bases are characterized by sharp and erosive contacts with a characteristic dark grey to black colour. The grading is supported by peaks in density values increasing from 1.4 to 2.0 g cm^{-3} at the base of the units. Gas cracks are identified in the homogenous parts of the facies, whereas the coarser base includes mica minerals. LF3 has been identified in four stratigraphic levels. LF4 shows normal grading with medium sand at its base (Fig. 10F). The base can be either erosive or conformable and contains organic matter, vivianite and mica. The units of LF4 are less than 10 cm thick, and have a density of 1.6 to 1.8 g cm^{-3} and magnetic susceptibilities of 40 to 110 × 10^5 SI. In the sediment core, 10 thicker layers (<10 cm) were detected with a medium sandy base and 43 very thin event layers (<2 cm) with a medium to fine sandy base (Figs 7 and 9).

Chronology

^{137}Cs radionuclide activity in the uppermost 30 cm of core SVA 12-1 highlights the occurrence of a well-defined and very strong peak at 3.25 cm (414 Bq kg^{-1}; Fig. 11). A second, smaller peak (167 Bq kg^{-1}) is detected at a depth of 5.75 cm (Fig. 11). The first peak is interpreted to coincide with the contamination induced by the Chernobyl nuclear reactor meltdown in 1986, whereas the second peak reflects the peak level of atmospheric nuclear weapon tests in the northern hemisphere in 1963 (Appleby, 2001). These interpretations agree with the fall-out data of soils in Europe following the Chernobyl accident (https://www.criirad.org/sommairecartessecteur/) and in

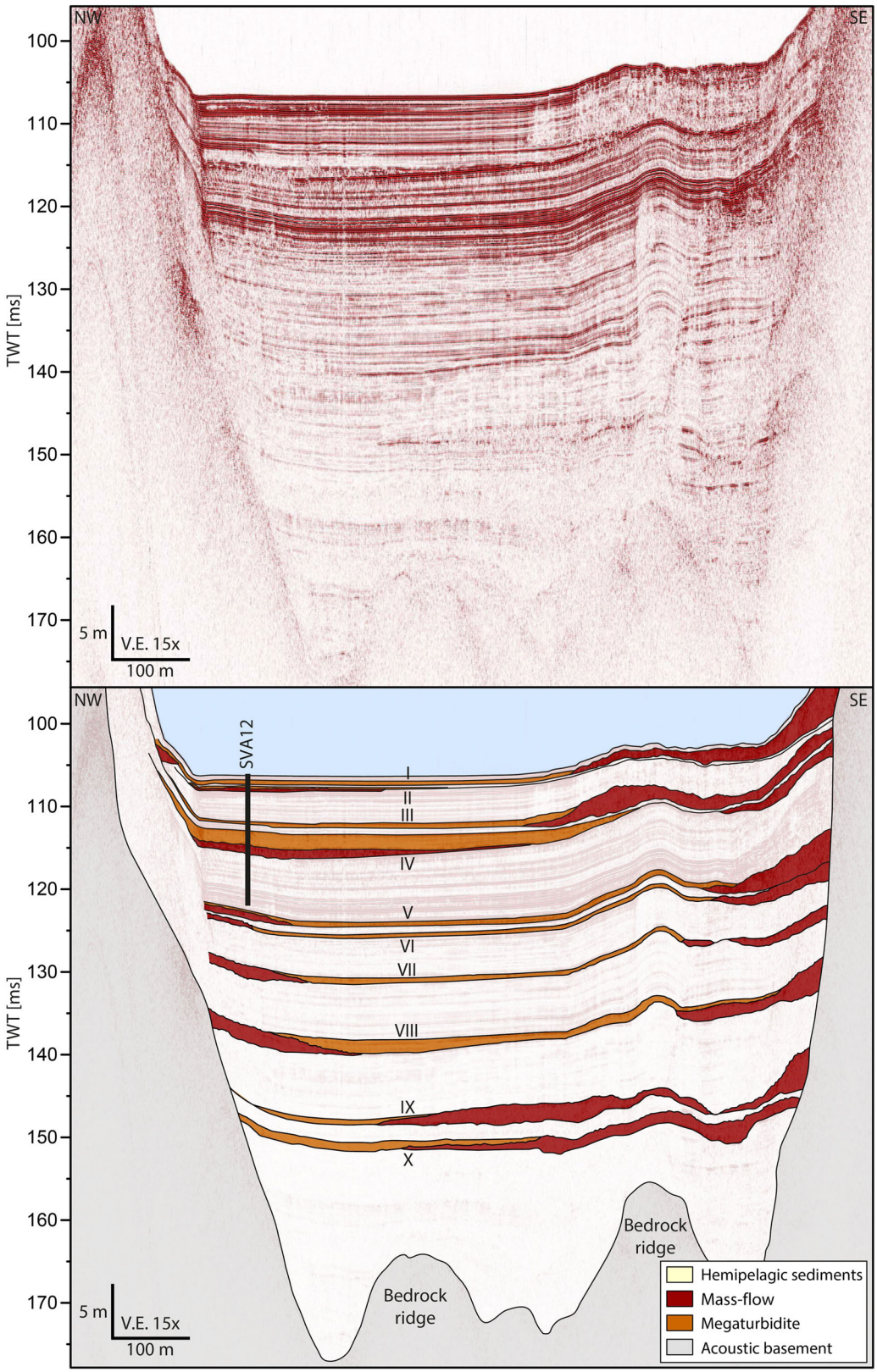

Fig. 7. Complete sediment infill with megaturbidites identified in the seismic stratigraphy indicating ten palaeoseismic events (I–X). Mass-flow deposits with wedging character (red) are always associated with a megaturbidite with onlapping character (orange). The black bar shows the sediment core SVA12. For profile location, see Fig. 3B.

sediments of Lake Tovel to the east of Lake Silvaplana (Kulbe *et al.*, 2005). The uppermost 6.5 cm of sediment of the short core were free of remobilized deposits (the first described turbidite occurs between 6.5 cm and 8.0 cm core depth). Including the suggested ages related to the ^{137}Cs peaks, an average background sedimentation rate of 1.2 mm a^{-1} was calculated for the time period of 1963 to 2012. Compared to the period of 1963 to 1986 with 1.1 mm a^{-1}, sedimentation rates for 1986 to 2012 seem to have slightly increased to 1.3 mm a^{-1}. The Bayesian age model for the core (Fig. 11) shows a sedimentation rate of 0.25 mm a^{-1} for the time period from 7700 to 3300 cal yr BP, 1 mm a^{-1} from 3300 to 1500 cal yr BP, 2 mm a^{-1} from 1500 to 200 cal yr BP, and 1 mm a^{-1} from 200 cal yr BP to present.

The timing of the 57 identified depositional events in the long core was established through the modelled age of the respective bottom depth of each event (Fig. 11; Table S1). Four event layers with multiple mass-flow wedges were recorded in the long sediment core and dated to 230 ± 45, 310 ± 65, 960 ± 160 and 1330 ± 90 cal yr BP. Furthermore, 53 smaller turbidite layers were cored, which occur more frequently during the last 4000 years. A radiocarbon date at the base of the sediment core revealed an age of 7661 cal yr BP.

INTERPRETATION OF STRATIGRAPHY

Comparing the seismic reflection patterns with lithological and physical properties of the sediment core enables an accurate seismic-to-core correlation (Fig. 12). The logs of the piston core show four lithological facies, which can be tied to the seismic facies. The continuous seismic reflections (SF1) correlate with the fine-grained laminations in the sediment core (LF1). These undisturbed units were interpreted as hemipelagic sediments, and the laminations formed by seasonal processes (Blass *et al.*, 2005, 2007a,b; Trachsel *et al.*, 2008, 2010; Stewart *et al.*, 2011a, b). Depending on prevailing climate and processes active in the catchment, the deposited laminations can vary in colour, porosity and stiffness (Gobet *et al.*, 2003). The bright laminations are identified in the hemipelagic sediments of the last 3300 years, and the dark laminations were deposited in the time period from 3300 to 7700 cal yr BP. A downcore change from bright varves to dark laminated sediments at *ca* 3300 cal yr BP is also observed in the sediment cores located at more shallow water depths of Lake Silvaplana (Leemann & Niessen, 1994).

The chaotic wedges correlate with deformed silty–clayey units, and the authors interpret these expressions as mass-flow wedges. Because sedimentology, density and susceptibility are all similar to the hemipelagic deposits, and former layering is still recognizable, the wedge-forming sediments were inferred to have failed in a cohesive behaviour ('mass flow'). Irregular lower boundaries indicate an erosive character of these mass flows. The upper boundaries are sometimes building up bulges, indicating folding and thrusting of the overridden and partly deformed basin-plain sediments during the emplacement of the mass-flow deposits (Schnellmann *et al.*, 2005; Sammartini *et al.*, 2021). This facies has also been recovered in previous studies by piston cores 90/1 and 90/2 (Fig. 13), but these sediments were not interpreted as mass-flow deposits (Leemann & Niessen, 1994). It is thus likely that there is no erosive contact related to these deposits when accumulated in the deepest part of the basin, and that the mass flows might consist of minimally deformed sediments of the Vallun Delta (Fig. 13; Leemann & Niessen, 1994).

The thicker normally graded units with a homogenous facies overlie the mass-flow wedges. These are interpreted as megaturbidite deposits related to the large suspension clouds produced during mass flows originating from overloaded steep lateral slopes and gently-dipping deltas. Megaturbidites are virtually instantaneous onsets of exceptionally large volumes of sediment (Bouma, 1987). The homogenous facies in the upper part of the megaturbidite is most likely formed by suspension settling following slope failure, as also observed in sediment cores from Hardangerfjord and the Corinth rift (Bellwald *et al.*, 2016a; De Gelder *et al.*, 2022). The colour of the megaturbiditic deposits is the result of mixing of fine-grained sediment settling in the water column. The sandy interlayers within the megaturbidite bed can be caused by seiche or other local mass-movement effects during the suspension settling. Large turbidity currents may be strongly erosive before becoming depositional (Sturm & Matter, 1978; Mulder & Cochonat, 1996). Compared to their thicker counterpart, the thinner normally-graded units are not overlying any wedges, and are interpreted as turbidites (Mulder & Cochonat, 1996). Although 53 of these turbidites have been cored, only the ten thickest of them can be recognized as a high-amplitude

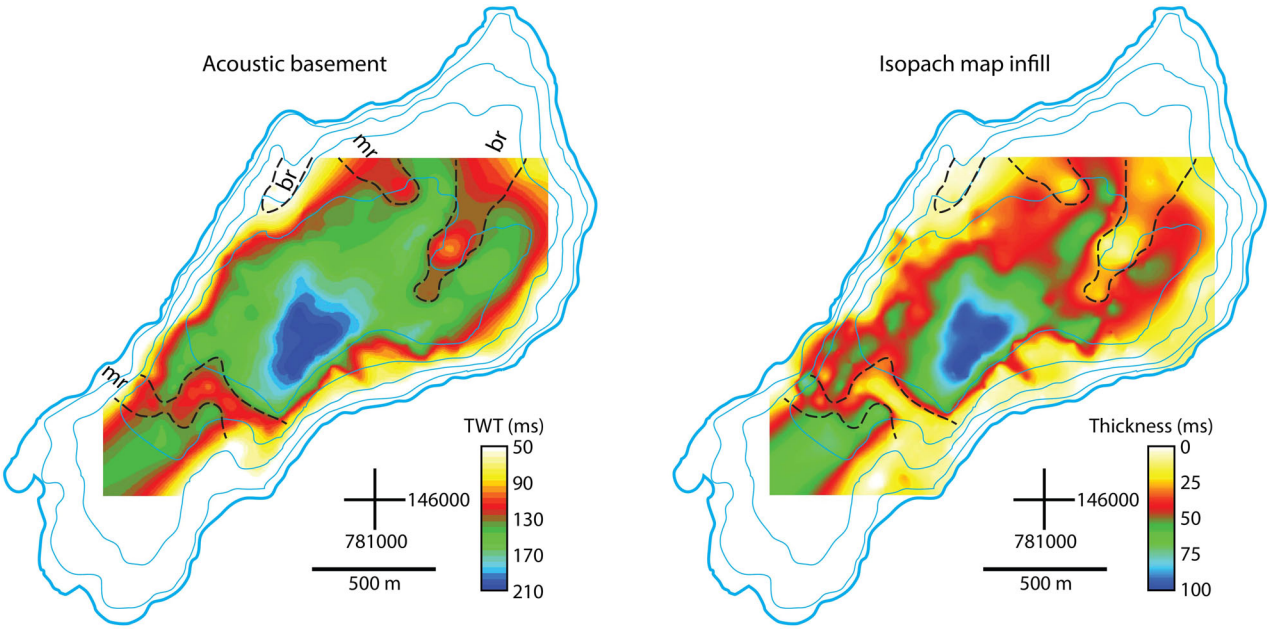

Fig. 8. Map of acoustic basement and infill of Lake Silvaplana. Two north-east/south-west (br: bedrock ridge) and two north-west/south-east oriented ridges (mr: moraine ridge) can be identified in the acoustic basement (extents indicated by dashed lines). These ridges are characterized by a thinner sediment overburden and form sub-basins. Blue lines indicate 20 m isolines of the modern lake bathymetry.

reflection in the seismic data, which can be related to vertical resolution of the pinger system (*ca* 10 cm). The authors infer settling of suspensive turbidity flows with smaller volumes and most likely local sources in their formation (Glur *et al.*, 2013; Wirth *et al.*, 2013; Støren *et al.*, 2016). A pronounced peak in magnetic-susceptibility data, high contents of organic matter and occurrence of vivianite indicate the origin of these turbidites to differ from the megaturbidites. Megaturbidites have not been described in piston cores 90/1 and 90/2 (Leemann & Niessen, 1994). Our seismic data indicate that there are no megaturbiditic deposits at these coring locations, but that the megaturbidites occur *ca* 200 m downslope of these sediment cores (Fig. 13).

The chaotic and heterogenous facies identified at the lower part of the seismic profiles (Fig. 7) is interpreted as acoustic basement, consisting either of glacial deposits or of crystalline bedrock. The top of this facies has successfully been mapped out for most of the lake (Figs 7 and 8). In areas with high gas content, the seismic signal did not image this facies boundary. Both glacial moraines and bedrock ridges are characterized by chaotic and transparent facies in the seismic data of lakes and fjords (Hilbe *et al.*, 2011; Bellwald *et al.*, 2016a,b; Fabbri *et al.*, 2018). The differentiation between glacial deposits and crystalline basement based on seismic facies interpretation in Lake Silvaplana is not possible. Using geomorphological criteria, the two lake-crossing ridges in the predominantly flat basin plain in the deep part of the lake more likely represent subaquatic moraine ridges and not outcropping bedrock ('mr' on Fig. 8). These subaquatic moraines formed along the front and sides of a glacier following the main valley, or ice masses originating from an elevated side valley. The two valley-following ridges expressed at the lake floor mirror the tectonic structure of the region, and are interpreted as bedrock ridges ('br' on Figs 3, 4, 8 and 13).

DISCUSSION

Stratigraphy of Lake Silvaplana

A deep basin and four ridges form the acoustic basement of Lake Silvaplana. The glacially overdeepened basin is *ca* 160 m (210 ms TWT) deep (with reference to lake level) and flanked by steep

Table 2. Facies description for the stratigraphy of Lake Silvaplana.

	Bright laminations *SF1, LF1a*	Dark laminations *SF1, LF1b*	Mass flow *SF2, LF2*	Thick turbidite *SF3, LF3*	Thin turbidite *SF3, LF4*
Seismic reflections	Continuous Moderate amplitudes		Chaotic Moderate-high amplitudes Irregular sharp upper and lower boundaries	Transparent Low amplitudes within turbidite sequence High amplitudes at lower boundaries	
Seismic character	Stratified Draping		Erosive Wedging Lobes	Onlapping Homogenous Ponding depressions	
Grain size	Laminated clay-silt		Deformed clay–silt	Coarse sand–fine sand/silt overlain by homogenous clay	Medium/fine sand
Sedimentology	Higher water content Absence of gas cracks	Sticky clay Lower water content Gas cracks	Patchy mottled pattern	Normal grading from coarse sand to fine sand/silt/clay Erosive base Presence of mica Gas cracks	Normal grading from medium sand to fine sand Both erosive and conformable Organic matter with vivianite at the base Presence of mica
Thickness (cm)	<1	*ca* 1	>10 or 1	>10	<10
Density (g cm^{-3})	1.4 (1.2–1.6)	1.5 (1.3–1.6)	1.4	1.4–2.0	1.6–1.8
MS (10^5 SI)	20–30	30	20	20–30	40–110
Process	Hemipelagic		Cohesive flow	Turbiditic flow	

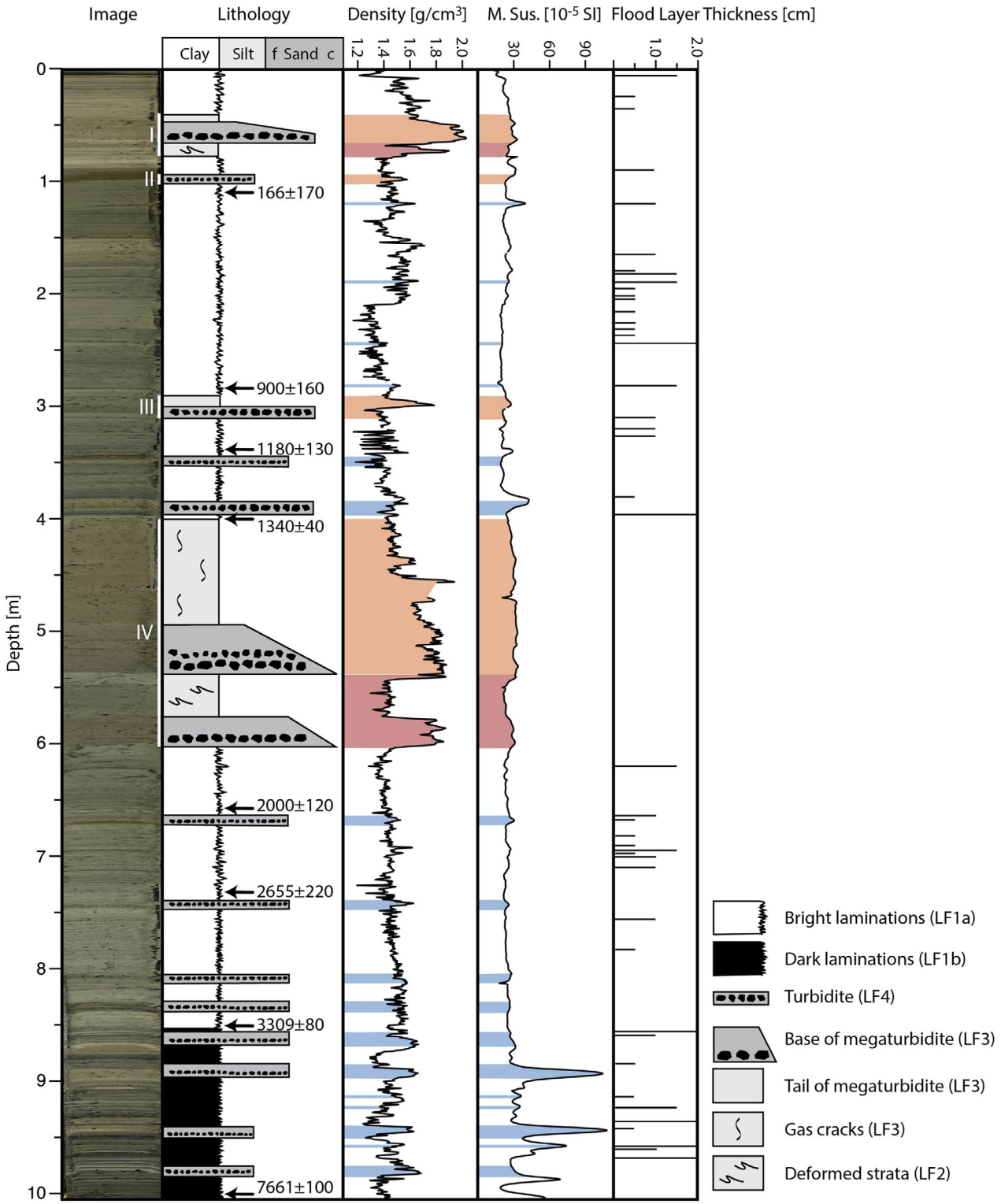

Fig. 9. Petrophysical properties of long sediment core (SVA12-2 and SVA12-3) plotted next to core photographs (with events I–IV indicated), lithological log with radiocarbon dates (arrows, in cal yr BP), density plot and magnetic susceptibility plot. Flood layers consisting of medium to fine sand with a thickness of less than 2 cm (in described intervals of 0.5 cm) are indicated to the right. Coloured bars show correlations of lithology to petrophysical properties with event layers (blue: flood-triggered turbidite, orange: earthquake-triggered megaturbidite, red: mass flow). M. Sus.: magnetic susceptibility, f: fine-grained sand, c: coarse-grained sand.

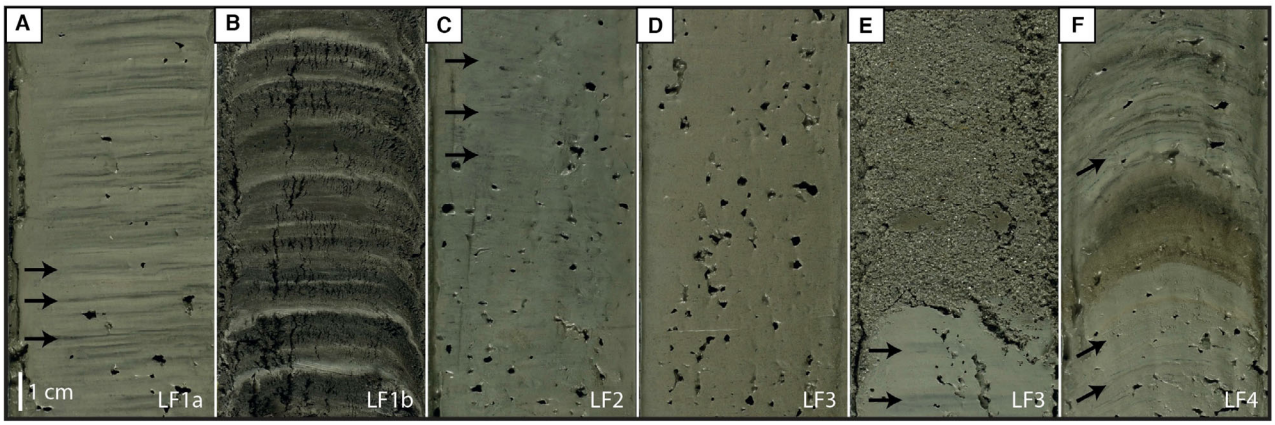

Fig. 10. Core photographs showing lithological facies (LF) identified in SVA12-2 and SVA12-3. (A) Bright laminations from the top of the core (LF1a, depth of 2.2 m in composite section). (B) Dark laminations from the base of the core (LF1b, depth of 10.0 m). (C) Deformed strata underlying megaturbidite. Former laminations are still weakly recognizable (LF2, depth of 5.7 m). (D) Centre of megaturbidite consisting of homogenous sediments (LF3, depth of 4.2 m). (E) Base of megaturbidite characterized by coarse-grained sand, erosive basal contact and mud-clasts (LF3, depth of 5.4 m). (F) Thin turbidite consisting of medium sand with smaller thickness and normal grading (LF4, depth of 6.7 m). Black arrows in core photographs indicate laminations.

slopes to the west and the east (Fig. 8). The two ridges at the lake floor have the same orientation as the Engadine Valley and follow the Engadine Line (Figs 1 to 3). Their formation might have been affected by the tectonic setting of the Engadine Valley. The two lake-crossing ridges formed smaller sub-basins in the Early Holocene, which became infilled and are no longer expressed on the modern lake floor. However, one of these ridges is associated with a slide scar along the gently-dipping lake floor (Figs 3A and 8), and might act as a location of slope instability. These lake-crossing ridges were interpreted as subaquatic moraines (see *Interpretation of stratigraphy* section); however, the seismic grid is not dense enough to make any more detailed conclusions about their formation.

Chironomids and pollen analysis at the Maloja Pass show that lakes existed in the Engadine Valley throughout the Late Glacial period, with strong input of glacial and/or snow meltwater and erosional input older than 13 700 cal yr BP (Ilyashuk *et al.*, 2009). Furthermore, the Egesen Stage moraines of the catchment glaciers are located upstream Lake Silvaplana (NFP 31, 1998) so that the lake was certainly ice-free before 12 800 cal yr BP. Therefore, lacustrine infill was suggested to have started with the onset of the Bølling-Allerød interstadial around 14 600 cal yr BP, and the moraines to be likely formed during the ice advance of the Gschnitz Stadial in the Late Glacial (*ca* 17 to 16 ka).

Rivers formed Gilbert-type deltas with gently-dipping slopes and limited acoustic penetration in the north-east and south-west. The reduced seismic penetration (4 ms in the Fedacla Delta) in these thick depocentres is most likely caused by the occurrence of free gas provided by the decomposition of organic material combined with the presence of coarse-grained, sandy sediments.

The postglacial sediment infill of Lake Silvaplana is characterized by ponding mass-movement deposits and draping hemipelagic sedimentation, resulting in an overall flattening of the basin floor. The highest sediment thickness of 75 m (100 ms TWT) is mapped in the deepest part of the basin, whereas the steep slopes show minimal sediment accumulation (Fig. 8). Stacked mass-flow deposits in the lake basin and mass-flow wedges at the toe-of-slopes and moraine flanks, combined with related deformation structures indicate repeated slope failures. The interpretation of the seismic data of Lake Silvaplana revealed multiple simultaneous mass-movement deposits at ten horizons of the sedimentary infill (labelled I–X; Figs 7 and 14). Mass-flow wedges originate from the steep western and eastern flanks, from delta environments (Vallun, Sagl, Rabgiusa), from acoustic-basement ridges and from the gently-dipping basin floor (Fig. 14). Thick megaturbidite deposits are onlapping the mass-flow wedges in the deepest basin. The megaturbidites

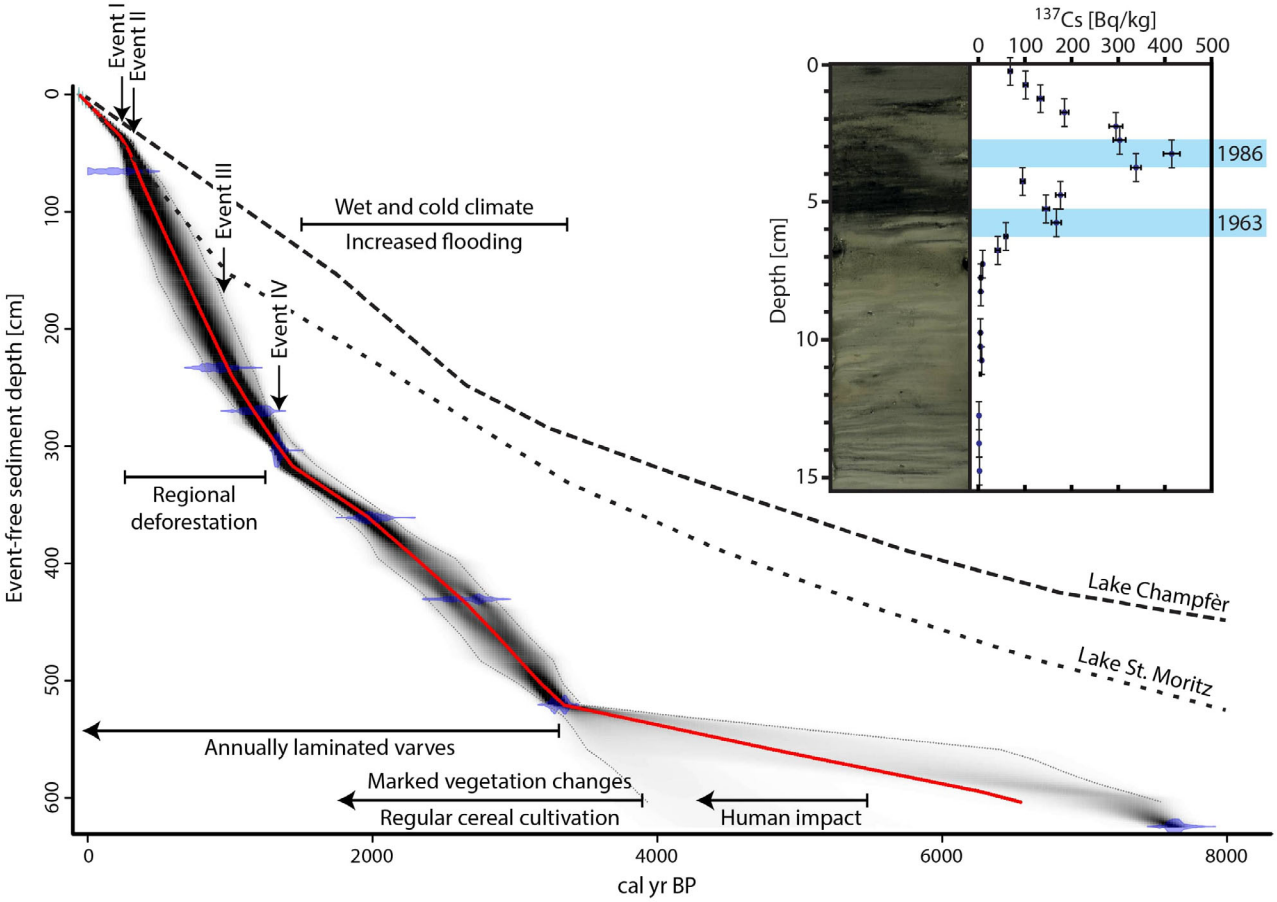

Fig. 11. Age model for the non-disturbed part of the sediment record (background sedimentation), excluding turbidite and mass-flow deposits. Crosses mark tie points in 2012 (top of core), as well as 1963 and 1986 defined by the ^{137}Cs analysis. Blue bars indicate the calibrated radiocarbon age with 2σ age distribution. The core reaches a basal age of 7661 cal yr BP. Age models from nearby Lake Champfèr and Lake St. Moritz from Gobet *et al.* (2003). Arrows show ages of earthquake-triggered events I to IV. Varves from Leemann & Niessen (1994), palaeoflooding from Stewart *et al.* (2011a), human impact, vegetation changes as well as regional deforestation from Gobet *et al.* (2003).

show similar depocentres for all the events with volumes of up to 292 000 m^3.

The Inn–Fedacla–Resgia deltas lack any large mass-flow deposits, but low seismic penetration cannot exclude their occurrence in the deeper surface. Cyclic steps expressed at the modern bathymetry (Fig. 4A), however, could indicate a more frequent small-scale mass transport or result from flood-driven underflows. Nevertheless, seismic reflection data provides evidence that delta failures repeatedly contributed to the large mass-movement deposits (Fig. 14).

Triggering mechanisms of mass movements

Multiple slide wedges were identified along ten horizons in the seismic data, four of which were cored and dated (Figs 9 and 14). Based on the distribution and stratigraphic location of the mapped mass movements, an external triggering mechanism is suggested for these deposits. Although deltas may fail spontaneously (Schnellmann *et al.*, 2005; Girardclos *et al.*, 2007), the observation that preferentially lateral slopes and the sediments above the ridge flanks are sliding, rules out delta collapses as the only origin for mass-flow development. Considering the presence of the Engadine Line, as well as historical and recent seismic activity in the region, the authors conclude earthquakes to be the most likely triggering mechanism for these simultaneously failed slopes.

Rapid sedimentation and gas charging are most likely the main preconditioning factors for slope

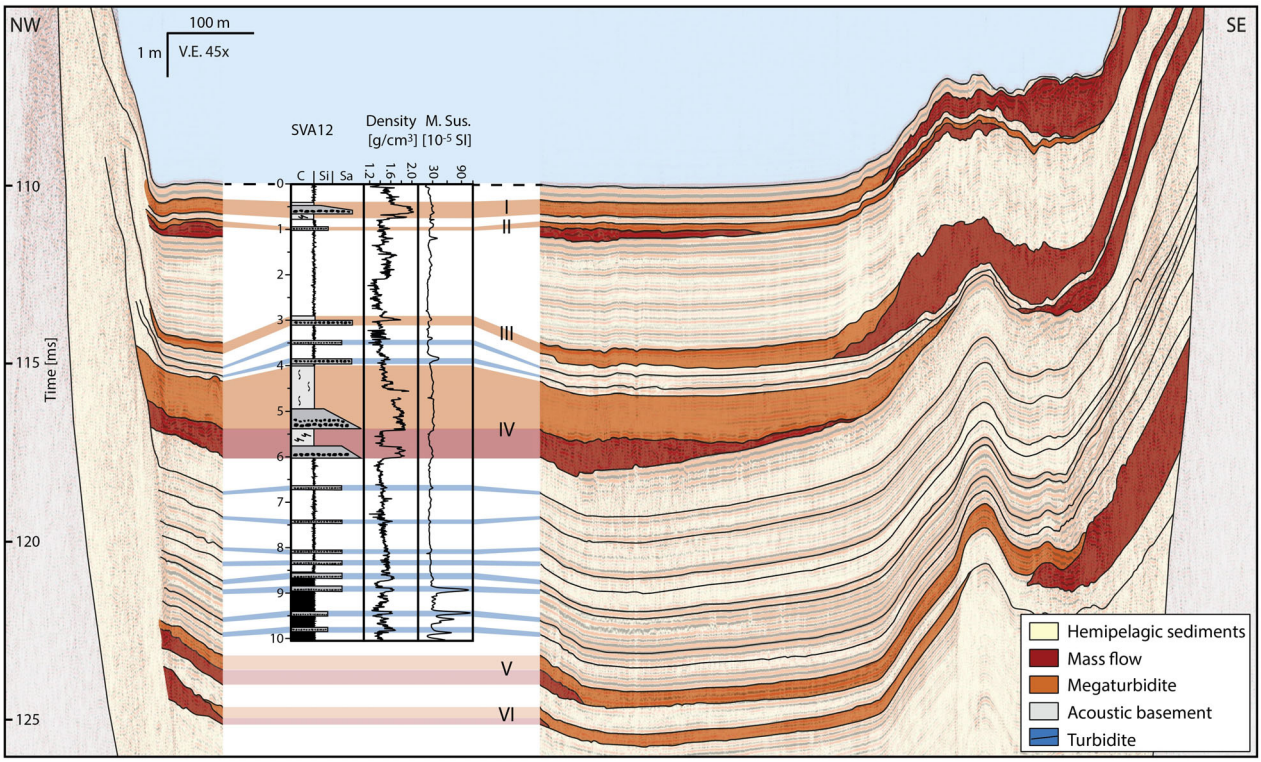

Fig. 12. Seismic-to-core correlation. Solid lines indicate the correlation between seismic stratigraphic event horizons and specific lithological beds. Core log includes lithological column and petrophysical properties (density and magnetic susceptibility) of the long sediment core SVA12. Four earthquake and ten flood events can be tied from the reflection seismic data into the sediment core. Flood layers larger than 2 cm commonly correlate with high-amplitude seismic reflections.

failure, because these processes can result in overpressure and a state of extreme underconsolidation (Lee, 2009; Schneider *et al.*, 2009; Wilhelm *et al.*, 2016; Bellwald *et al.*, 2019b). The age model of Lake Silvaplana shows an association between slope failure and increased sedimentation rates (Fig. 11), but slope failures did not occur for 1900 years compared to increased sediment accumulation from *ca* 3300 cal yr BP onward. The threshold for slope instability might depend on sediment preconditioning related to sedimentation rate (Wilhelm *et al.*, 2016) and existing overpressure. The first pulse of increased sedimentation (average of 1.2 mm a^{-1}) at *ca* 3300 cal yr BP did not result in any slope failures, thus excluding sediment loading alone as the dominant triggering mechanism. The second pulse of increased sedimentation (average of 2.2 mm a^{-1}) at *ca* 1400 cal yr BP, however, shows a strong association with basin-wide slope failure (Fig. 11).

The 53 smaller turbidites with a fine to medium sandy base have been described in core data, and ten of them correlate with a high-amplitude reflection in the seismic data (Fig. 12). Seismic-to-core correlation further shows an increase in density and magnetic susceptibility in the thicker of these beds. Unlike megaturbidites, these reflections do not correlate with any mass-wasting wedges, and are commonly draping existing topography. Lacustrine studies from different areas of the Alps related these thin layers with a sandy base and gradation, as well as excursions in magnetic susceptibility values, to the development of flood events producing turbiditic underflows (Sturm & Matter, 1978; Sturm *et al.*, 1995; Chapron *et al.*, 2002, 2005; Støren *et al.*, 2010; Gilli *et al.*, 2013; Glur *et al.*, 2013; Wirth *et al.*, 2013). Following these interpretations, the 53 thin turbidites identified in the long sediment core were suggested to represent flood deposits consisting of catchment-sediment remobilized and delivered through overland runoff into the lake during: (i) high-precipitation events; and (ii) from increased glacial activity, i.e. a glacial outburst flood (Vandekerkhove *et al.*, 2021).

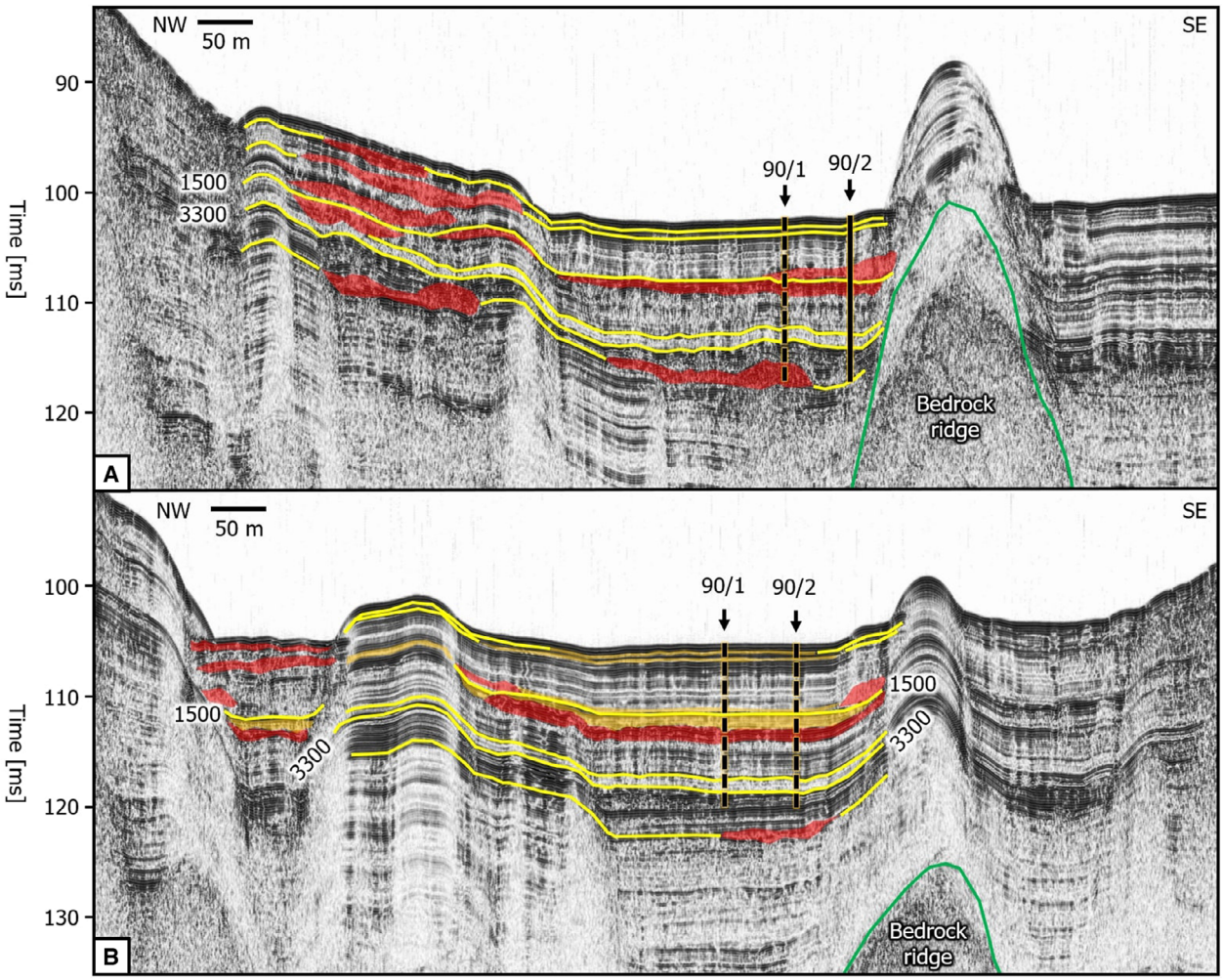

Fig. 13. Lateral changes in stratigraphy, sediment thickness and occurrence of event deposits in the Vallun Delta with suggested ages of the seismic reflections based on age model of piston core 90/2 (Leemann & Niessen, 1994). (A) Most proximal seismic profile across the Vallun Delta. Yellow lines are seismic stratigraphic key reflections for correlation of our dataset. Mass-flow deposits (orange), megaturbidites (golden) and top acoustic basement (green line) are shown. Sediment core 90/1 is located in a distance of *ca* 100 m upslope, and are projected onto the seismic profile. (B) More distal seismic profile across the Vallun Delta. Piston cores 90/2 and 90/1 (Leemann & Niessen, 1994) are located *ca* 200 m and 300 m upslope of the seismic profile, respectively, and are projected onto the seismic profile. For profile location, see Fig. 3B.

Snowmelt in spring is negligible in Lake Silvaplana (Blass *et al.*, 2007b).

Flood turbidites may have a duration of several days, and the fining-upward sequence reflects the waxing and waning of the discharge (Sturm & Matter, 1978). Peaks in magnetic susceptibility are attributed to the concentration of allochthonous magnetic minerals frequently occurring in flood deposits (Gilli *et al.*, 2013; Støren *et al.*, 2016). As shown for other Alpine lakes (Czymzik *et al.*, 2013; Swierczynski *et al.*, 2013; Wirth *et al.*, 2013), Lake Silvaplana therefore can also be used as a climate archive recording major flood events. Smaller flood events, however, might only be recorded in the delta environment of Lake Silvaplana, and not have left any evidence in its deepest basin.

Delivery of detrital materials through riverine input is crucial for sediment availability and slope gradient, and sediment overloading at oversteepened slopes could act as the main preconditioning factor for slope failure in the deltas. All ten major events show slide wedges originating from the major deltas (Vallun, Sagl and Rabgiusa), which requires sediment recharging. Cyclic steps in the south-west of the lake

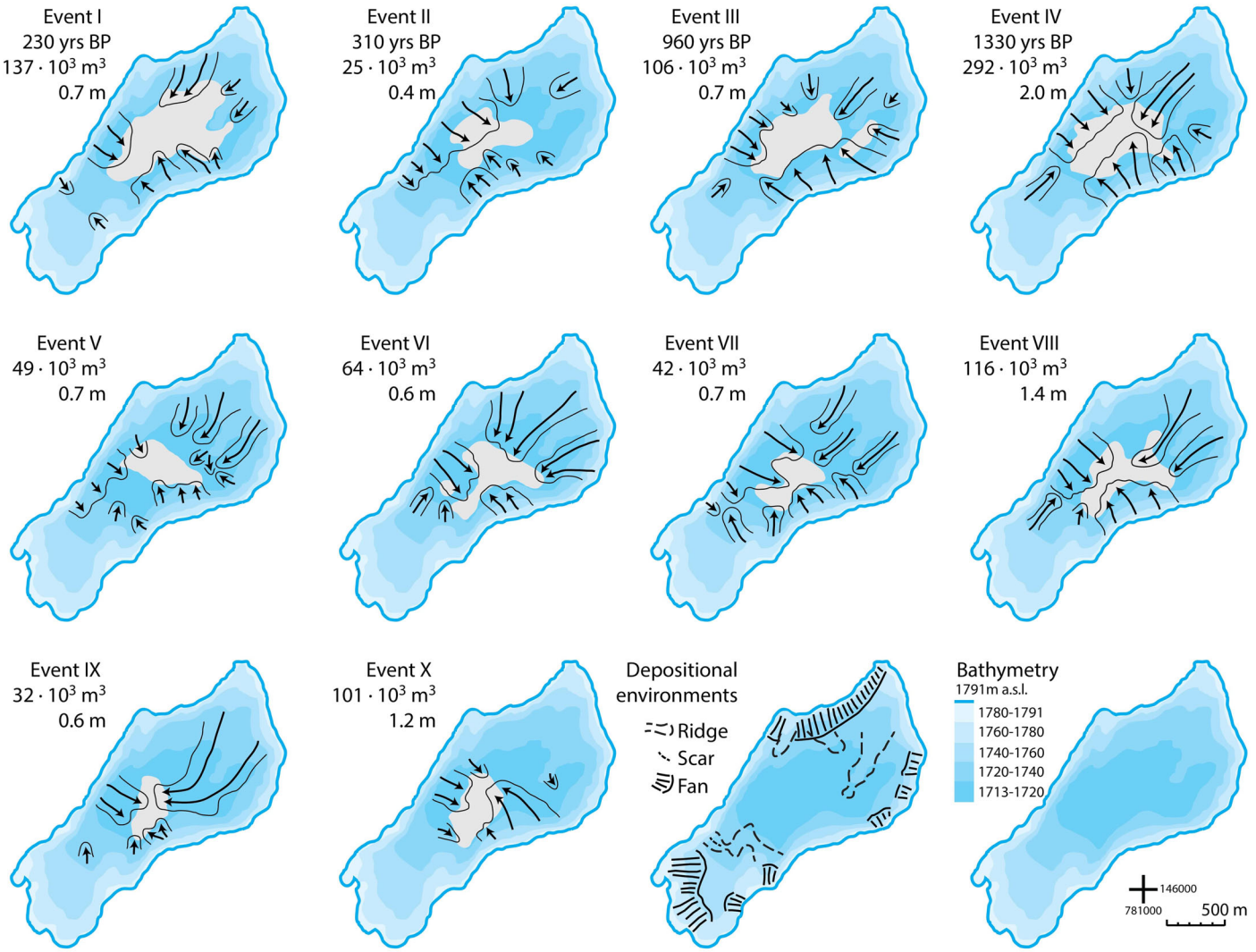

Fig. 14. Spatial distribution of 10 earthquake event layers characterized by multiple mass movements identified in the seismic data. Maps showing simultaneous multiple mass-flow deposits (black-lined areas) with possible trajectories (black arrows) in Lake Silvaplana for 10 suggested palaeoearthquakes. Grey areas mark the extent of megaturbidite deposits associated with these mass flows. Volume and maximal thickness of each event layer is reported in the top left corner of each map. Event I: 231 cal yr BP [184 to 273; 1719 CE (1766 to 1677)]; Event II: 307 cal yr BP [244 to 372; 1643 CE (1706 to 1578)]; Event III: 962 cal yr BP [812 to 1135; 988 CE (1138 to 815)]; and Event IV: 1332 cal yr BP [1285 to 1468; 618 CE (665 to 482)]. Pre-dated events V to X are older than 7661 cal yr BP. Lake floor and depositional environment based on bathymetric data are shown at the bottom right.

indicate more frequent, small-scale mass movements or flood-triggered underflows for the Inn, Fedacla and Resgia deltas. These rivers are dominated by glaciated catchments, and the presence of glaciers might be critical for sediment delivery and formation of cyclic steps. The present study did not identify any major slide escarpments in the bathymetric data nor detect any slide wedges originating from the Inn and Fedacla deltas. The sediments provided by the Inn and Fedacla rivers might thus have been directly transported to the deeper basin, and the overload could explain the large slide escarpment in the basin (Fig. 4A). A very similar relationship between glaciated catchment, cyclic steps and large slide escarpments has been documented from the largest delta of Hardangerfjorden, west Norway (Bellwald *et al.*, 2016b).

Sedimentation patterns

Our age model suggests sedimentation rates of 0.2 mm a^{-1} for the mid-Holocene (7700 to 3300 cal yr BP), 1.2 mm a^{-1} for the first part of the Late Holocene (3300 to 2000 cal yr BP), 0.9 mm a^{-1} for the period from 2000 to 1400 cal yr BP and 2.2 mm a^{-1} for the last 1400 years. The sedimentation rate in the period from 2000 to 1400 cal yr BP could be a minimum value for the sediment accumulation, as parts of the record might have been eroded during Event IV. Previous studies from more proximal environments of Lake Silvaplana yielded slightly higher sedimentation rates: A study based on a core collected between the Vallun Delta and the deepest basin described an average couplet (varve) thickness of 1.4 mm for the period of 2500 to 1830 cal yr BP (570 BCE to 120 CE; Stewart *et al.*, 2011b). Because our long core has been recovered from the deepest basin, a sedimentation rate of 1 mm a^{-1} is reasonable (Fig. 3B). The increase in sediment accumulation at *ca* 3300 cal yr BP is also observed in the piston cores analysed by Leemann & Niessen (1994).

A change in lithological facies was observed from dark laminations before *ca* 3300 cal yr BP to bright laminations afterwards (Figs 9 and 10). A transition from sediments with significantly higher organic content into varves of bright colour has also been observed by Leemann & Niessen (1994) in Lake Silvaplana. Such a change correlates with the sediments of Lake St. Moritz, where dark gyttja is deposited until 4000 cal yr BP, followed by bright gyttja in the more recent millennia (Gobet *et al.*, 2003). This lithological change correlates with an increased sedimentation rate in Lake Silvaplana, Lake Champfèr and Lake St. Moritz. However, the increase in sediment supply is more significant in Lake Silvaplana compared with Lake Champfèr and Lake St. Moritz (Fig. 11). The Late Holocene is characterized by a wetter and colder climate in the region (Gobet *et al.*, 2003; Stewart *et al.*, 2011b). The authors suggest that the more extensively glaciated catchment of Lake Silvaplana resulted in a stronger signal in the sedimentary record of Lake Silvaplana compared to the lakes in the north-east. Lauterbach *et al.* (2012) identified a significant increase in sedimentation at *ca* 2500 cal yr BP for Lake Iseo, *ca* 70 km to the south of the study area. The change in sedimentation from low rates in the mid-Holocene to high rates in the Late Holocene has been observed in many lakes of the Alps (Leemann & Niessen, 1994; Ohlendorf *et al.*, 1997; Blass *et al.*, 2007b; Giguet-Covex *et al.*, 2011; Nussbaumer *et al.*, 2011; Czymzik *et al.*, 2013), as well as in lakes and fjords with glaciated catchments within the northern hemisphere (Vasskog *et al.*, 2011; Bellwald *et al.*, 2016a, 2019a).

Changes in sedimentation rates in the Late Holocene can have multiple causes: Strong human activity in the Engadine Valley from around 5500 cal yr BP changed the vegetation in the catchment. Forests were reduced and meadows enlarged, leading to pastured woodlands, the so-called 'larch-meadows' (Zoller & Brombacher, 1984; Gobet *et al.*, 2003). Soil erosion and thus terrigenous supply was consequently enhanced (similar in Chapron *et al.*, 2002, Lake Le Bourget). Marked vegetation changes and regular cereal cultivation started *ca* 3900 cal yr BP (Gobet *et al.*, 2003). Evidence for regional deforestation was found in pollen and charcoal data from sediments of Lake St. Moritz between 700 to 1700 CE (Gobet *et al.*, 2003). Coarser-grained, darkly-laminated sediments with low sedimentation rates indicate an absence of glacial meltwater input into Lake Silvaplana from 7700 to 3300 cal yr BP. In contrast, more fine-grained and brightly-laminated sediments correlate with an increased glacier and flood activity in the Late Holocene.

Chronology of event deposits

The upper four earthquake-triggered mass movements (I–IV) were dated between 230 and 1330 cal yr BP, whereas the age of the six earthquake-triggered mass movements in the

deeper stratigraphy (V–X) cannot be well-constrained (Fig. 15). The base of the core at *ca* 7700 cal yr BP is the minimum age for these events, whereas the deglaciation of the area around *ca* 14 600 cal yr BP is a maximum age (Ivy-Ochs *et al.*, 2008; Ilyashuk *et al.*, 2009). The chronology of the earthquake-triggered mass movements shows that the last 1400 years were seismically more active compared to the interval between 1400 to 7700 cal yr BP, for which the authors did not document any seismic events in the stratigraphy of Lake Silvaplana (Fig. 15). The pronounced seismic cluster of the Late Holocene, with Events I to IV, does not correlate with clusters in the compilation of earthquake-induced mass movements of Switzerland (Kremer *et al.*, 2017, 2020a), indicating that the Engadine Valley might have an independent palaeoseismic history.

In addition to the ten megaturbidites, 53 thinner turbidites have been identified in the sediment core and partly by high-amplitude reflections in the seismic profiles, which are interpreted as flood events. Our study shows an increased flood activity for the periods of 3400 to 2900, 2600 to 2000 and 1500 cal yr BP to present, with individual thicker layers at 7100, 6100, 4200 and 3700 cal yr BP (Table S1). Our observed clusters in flood activity correlated with the onset of varves (Leemann & Niessen, 1994) as well as wet and cold climate in the region (Stewart *et al.*, 2011a). The increased flood activity from 2600 to 2000 cal yr BP of our study coincides with increased flood activity documented by Stewart *et al.* (2011a). In contrast to Leemann & Niessen (1994) and Stewart *et al.* (2011a,b), this study did not identify any floods between 1950 to 1420 cal yr BP, although these deposits might be eroded by the thick slide wedge dated to 1330 cal yr BP. The last cluster of high flood activity (1500 cal yr BP to present) comprises the four cored, earthquake-triggered mass movements. Increased flood-induced sedimentation rate might have preconditioned slope stability and increased the sensitivity of slopes towards failing. Moreover, at the same time, Gobet *et al.* (2003) suggest regional deforestation in the area also contributing towards increased particle flux. However, sedimentation rate alone cannot explain the identified mass movements on the lateral slopes as they still require earthquake-triggering to be released.

Earthquake record and regional correlation

The most recent megaturbidite in Lake Silvaplana, dated to 1719 CE (1677 to 1766 CE) and defined as Event I (Fig. 7), onlaps three large and six small coeval mass-flow deposits originating from different slopes and the Vallun Delta (Fig. 14). A volume of 137 000 m^3 and a maximum thickness of 0.7 m makes this megaturbidite the second largest of the 10 megaturbidite deposits detected in the seismic data. The closest candidate listed in the Swiss earthquake compilation (ECOS-09, 2011) correlating with our postulated event is the Mw *ca* 5.0 Prättigau earthquake in 1695 CE, located *ca* 50 km north of Lake Silvaplana (Fig. 16A). However, there are multiple historic earthquakes correlating with the age interval of Event I, and it is challenging to define which earthquake caused these mass movements.

The megaturbidite characterizing Event II comprises of a volume of 25 000 m^3 and a maximum thickness of 0.4 m. The dimensions of the megaturbidite are consequently the smallest of the 10 events. The mass flows of Event II mainly originate from the lateral slopes, while most of the deltas have been stable. The event is dated to 307 cal yr BP (median of 1643 CE, interval of 1578 to 1706 CE), and potentially might correlate to three historic earthquakes: (i) the Mw *ca* 4.4 earthquake in Chiesa (northern Italy) in the year 1623 CE, located *ca* 20 km in the south of Lake Silvaplana; (ii) the Mw *ca* 5.0 Bergamo earthquake in 1642 CE (*ca* 80 km south of our study site; ECOS-09, 2011); or (iii) most likely, to the Mw *ca* 5.4 Ftan earthquake in 1622 CE, only 50 km to the east of Lake Silvaplana (Fig. 16B). Event II further coincides roughly with trees located in shallow water depths in the southwest of Lake Silvaplana that are radiocarbon dated to 1450 to 1650 CE (Schlüchter *et al.*, 2018; Fig. 2), implying that these trees could have been redeposited by a mass movement triggered by the suggested earthquake.

Event III consists of eight coevally-triggered mass flows originating from different lateral slopes, the Vallun and Sagl deltas, and one from the gently-dipping basin. It is characterized by a maximum thickness of 0.7 m and a calculated volume of 106 000 m^3. Event III is dated to 962 cal yr BP (812 to 1135 cal yr BP), and occurred in between 815 to 1138 CE (Fig. 16C). Thus, it fits with the Mw *ca* 5.2 earthquake in Brescia (*ca* 100 km to the south) in 1065 CE (ECOS-09, 2011), the Middle Adige Valley earthquake in 1046 CE (Guidoboni & Comastri, 2005; Guidoboni *et al.*, 2007; *ca* 110 km to the south) and the Verona Mw *ca* 6.5 earthquake in 1117 CE (Guidoboni *et al.*, 2005; *ca* 150 km to

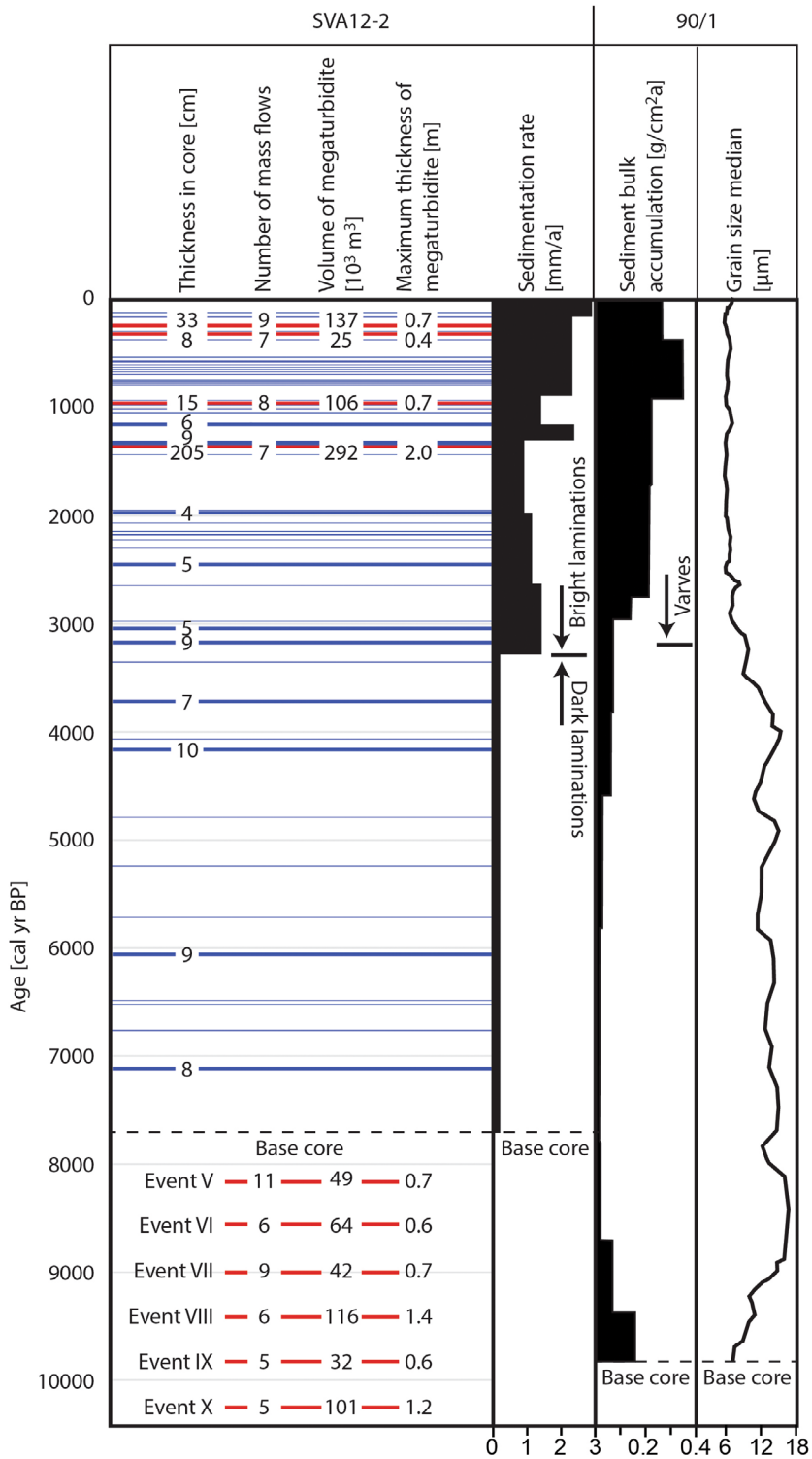

Fig. 15. Event catalogue of Lake Silvaplana with earthquake-triggered and flood-triggered turbidite layers, and background sedimentation rate. Horizontal thick bars indicate earthquakes (red) and floods (blue) identified in both seismic and sediment-core data. Horizontal thin bars indicate floods <2 cm only identified in the sediment core, which reaches to 7661 cal yr BP. Red bars below base core are the six coeval mass movements not cored (V–X). The number of mass flows is based on the spatial distribution maps in Fig. 14. Sedimentation rate from this study, and sediment bulk accumulation as well as grain-size median of Lake Silvaplana from Leemann & Niessen (1994).

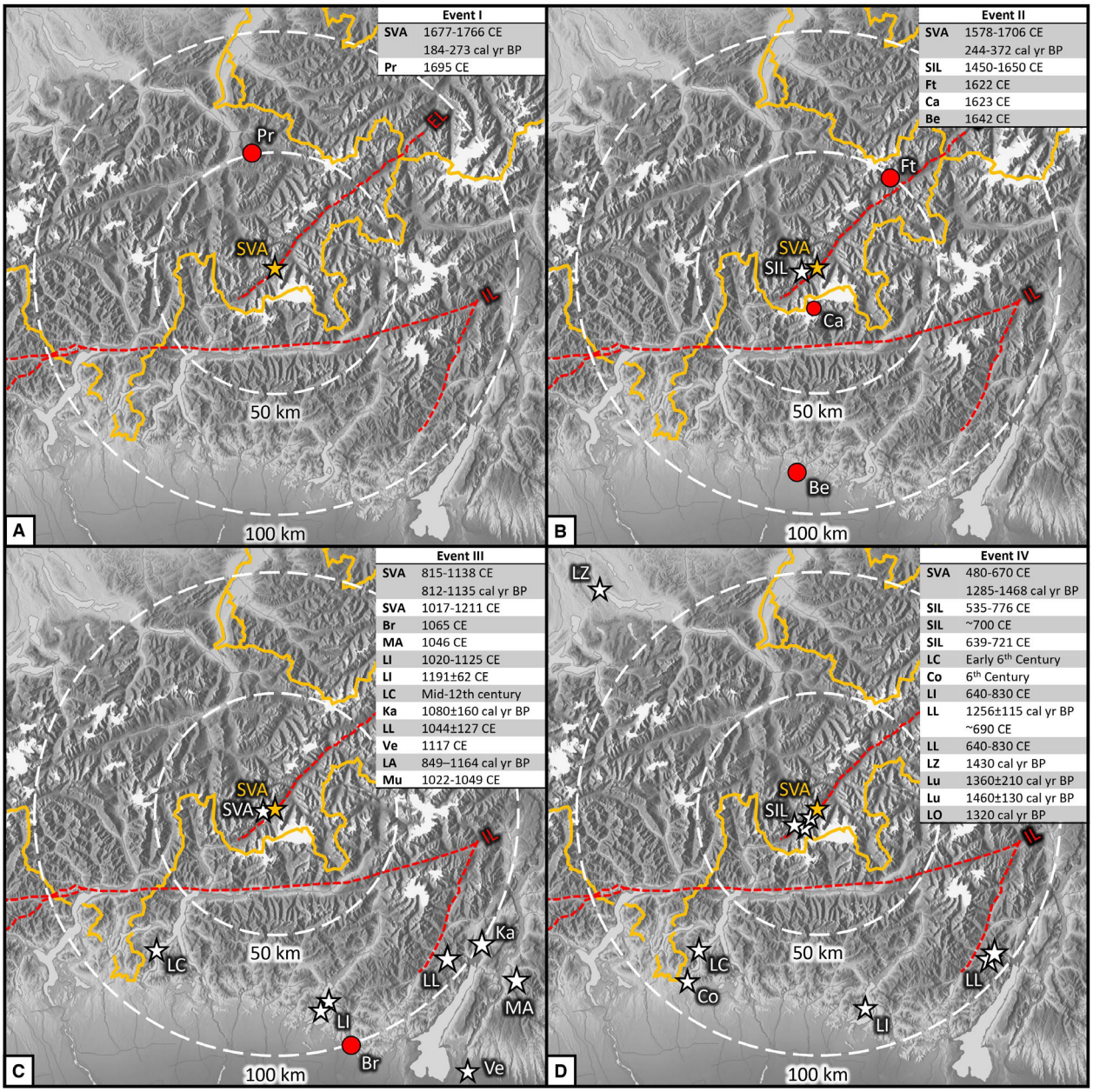

Fig. 16. Regional overview of Events I to IV (a–d). Shown are tectonic elements (red dotted lines), sedimentary archive of this study (golden star), associated historical earthquakes (red dots) and associated sedimentary deposits (white stars). Be: Bergamo, Br: Brescia, Ca: Chiesa, Co: Como, EL: Engadine Line, Ft: Ftan, IL: Insubric Line, Ka: Kas, LA: Lake Achensee, LC: Lake Como, LI: Lake Iseo, LL: Lake Ledro, LO: Lake Oeschinen, Lu: Lake Lungern, LZ: Lake Zurich, MA: Middle Adige Valley, Mu: Münster, Pr: Prättigau, SIL: Lake Sils, SVA: Lake Silvaplana, Ve: Verona. Lake Achensee is located *ca* 180 km north-east of Lake Silvaplana, rock avalanche of Münster is located *ca* 190 km east of Lake Silvaplana, Lake Lungern is located *ca* 130 km north-west of Lake Silvaplana, and Lake Oeschinen is located *ca* 160 km west of Lake Silvaplana.

the south). Fanetti *et al.* (2008) estimated the age of a likely earthquake-triggered megaturbidite with a volume of 3×10^6 m^3 in Lake Como around the mid-12th century. Earthquake-triggered mass movements related to the Brescia earthquake have also been identified in Lake Iseo, *ca* 70 km to the south, and dated to 1020 to 1125 CE (Rapuc *et al.*, 2022). The Kas rock

avalanche, dated to 1080 ± 160 cal yr BP, is suggested to be triggered by the Middle Adige Valley earthquake at 1046 CE (Ivy-Ochs *et al.*, 2017). A seismic trigger has also been postulated for a mass movement in Lake Ledro, dated to 1044 ± 127 CE (Simonneau *et al.*, 2013). A turbidite in Lake Achensee, located *ca* 180 km north-east from Lake Silvaplana, has been dated to 849 to 1164 cal yr BP, and has been suggested to be triggered by a remote earthquake (Oswald *et al.*, 2021). Further evidence supporting an over-regional trigger mechanism at the postulated time in Lake Silvaplana are *in situ* and fallen trees, observed during a diving expedition in 2005 at a depth of about 20 m and dated by radiocarbon to the beginning of the 11th century (1017 to 1211 CE; Schlüchter *et al.*, 2018; Fig. 2). A likely explanation for the trees identified in the subaquatic domain could be downslope transport by an earthquake-triggered mass movement. In addition, the rock avalanche of Münster (Inn Valley, Eastern Alps, *ca* 190 km east of Lake Silvaplana) is dated to 1022 to 1049 CE (Sanders *et al.*, 2021), and also correlates with the age interval of Event IV.

Event IV is the largest earthquake-triggered megaturbidite and characterized by extensive slide wedges originating from four unconnected slopes and the gently-dipping basin floor, resulting in an up to 2 m thick megaturbidite with a volume of 292 000 m^3. The event is dated to *ca* 620 CE (480 to 670 CE; 1285 to 1468 cal yr BP). This event coincides within radiocarbon resolution with the most prominent mass-movement deposit in neighbouring Lake Sils (Fig. 16D), where an up to 6 m thick megaturbidite with a volume of 6.5 × 10^6 m^3 is radiocarbon dated to 535 to 776 CE (Blass *et al.*, 2005). A related clastic deposit in the shore and nearshore area has further been interpreted as a tsunami deposit related to the same delta collapse in the south-eastern part of Lake Sils (Nigg *et al.*, 2021; Fig. 2). Furthermore, seven radiocarbon dates of trees standing in water depths of *ca* 30 m in the south-west of Lake Sils indicate median ages of 639 to 721 CE (Schlüchter *et al.*, 2018). In Lake Como, roughly 90 km from our study site, a prominent lacustrine mass movement was dated to the early 6th century and also suggested to be earthquake-triggered (Fanetti *et al.*, 2008). An undocumented earthquake in the 6th century has been suggested based on deformations in a stratigraphic sequence and in an archaeological site in Como city (Livio *et al.*, 2023). Livio *et al.* (2023) claim a minimum Mw 6.32 earthquake with an epicentre located at the border between Italy and Switzerland to have triggered slope failure and deformation in different archives. Submarine mass movements in Lake Ledro (*ca* 100 km south-east) have been dated to 1256 ± 115 cal yr BP (*ca* 690 CE; Simonneau *et al.*, 2013) and to 640 to 830 CE in Lake Iseo (*ca* 70 km to the south; Rapuc *et al.*, 2022). Evidence from archives located with a distance larger than 100 km include: (i) a bed with coeval slope failure dated to 1430 cal yr BP in Lake Zurich (*ca* 520 CE; Strasser *et al.*, 2013); (ii) two mass movement deposits dated to 1360 ± 210 cal yr BP in Lake Lungern (*ca* 590 CE; Monecke *et al.*, 2006); and (iii) a mass movement dated to *ca* 1320 cal yr BP in Lake Oeschinen (*ca* 630 CE; Knapp *et al.*, 2018). All of these studies support our interpretation for a single earthquake to trigger these mass flows. Thus, it is postulated here that a catastrophic event in the early 7th century, caused by an over-regional, large earthquake involving cascading events, was able to trigger all of the documented deposits. Although only indirectly indicative for a seismic trigger, the megaturbidite volume is by far the largest cored and mapped in Lake Silvaplana (Fig. 14). As associated slope failure extends from Lake Zurich in the north to Lake Como in the south, with strong evidence in different archives of the Engadine Valley, the earthquake might have had an epicentre close by (Fig. 16D). Although Albini *et al.* (1988) claim that the Engadine Line is seismically active in recent times, signals of direct neotectonic activity, as expressed in faults, have not been observed in seismic data so far.

The combined effects of the postulated earthquake, the delta collapse and the following tsunami provide an explanation for the coarse-grained layer overlying a peat layer and burying Roman altars in Sils-Maria (Erb *et al.*, 1966). Numerical simulation shows that the tsunami waves that were generated from the delta collapse in Lake Sils had an overflow into Lake Silvaplana (Nigg *et al.*, 2021). However, it is unlikely that the tsunami wave could have caused basin-wide lateral slope failure in Lake Silvaplana, especially as this study also identified a failure scar in the deep basin (Fig. 3A).

The cluster of six regionally-triggered mass movements between 11 300 and 7700 cal yr BP (Events V–X; Fig. 15) might be related to the deglacial history of the Engadine Valley. Enhanced mass movement activity following deglaciation is also observed in other lakes in the

Alps (Beck *et al.*, 1996; Monecke *et al.*, 2006; Schnellmann *et al.*, 2006; Simonneau *et al.*, 2013; Strasser *et al.*, 2013; Oswald *et al.*, 2021) and Norwegian fjords (Böhme *et al.*, 2015; Hermanns *et al.*, 2017; Bellwald *et al.*, 2019a). The time periods from 10 to 9 and 2 to 1 cal kyr BP are characterized by increased slope instabilities in the Alps (Ivy-Ochs *et al.*, 2017). Rock avalanches, suggested to have a link with enhanced crustal seismicity by glacio-isostatic rebound, are documented throughout the Early Holocene (Ivy-Ochs *et al.*, 2017). The six seismically-triggered mass movements, Events V to X, all occurred between 7700 to 11 300 cal yr BP. This time period of Events V to X further correlates with a cluster of enhanced seismic activity in the Swiss earthquake catalogue (Kremer *et al.*, 2017). The compilation of rock avalanches shown by Ivy-Ochs *et al.* (2017) lists several candidates that could potentially be, similar to the mass movements in Lake Silvaplana, secondary effects of large earthquakes in Eastern Switzerland or northern Italy. Sedimentation rates in Lake Champfèr and Lake St. Moritz are strongly increased for the time period from 11 000 to 11 500 cal yr BP (Gobet *et al.*, 2003), and might have contributed to the volumes and enhanced susceptibility of the Early-Holocene mass movements.

Events V and VI are located 1 and 2.5 ms TWT below the base of the long sediment core, respectively, and are thus somehow older than the basal core age of *ca* 7700 cal yr BP (Figs 6 and 7). One of these events might correlate to the largest mass movement detected in neighbouring Lake Champfèr, which occurs close to the seismic reflection dated to *ca* 7700 cal yr BP (Gobet *et al.*, 2003; Fig. 17).

Sensitivity of Engadine lakes to register tectonic and climatic changes

Sensitivity for seismically-triggered mass movements

A comprehensive comparison with other palaeoseismic archives of south-eastern Switzerland and northern Italy was conducted to establish a more complete and reliable palaeoearthquake record with the earthquake reconstruction from Lake Silvaplana (Fig. 16). Event III is the best case to discuss earthquake-signal recording within the sediments of Lake Silvaplana. The suggested age of 815 to 1138 CE allows three earthquakes, all with epicentres in northern Italy, as potential seismic trigger for this mass movement: The Brescia earthquake in 1065 CE, the Middle Adige Valley earthquake in 1046 CE and the Verona earthquake in 1117 CE. The Brescia earthquake (Mw *ca* 5.2) was suggested as the most likely candidate, because it is located 100 km south from Lake Silvaplana compared to the 150 km distance of Verona (although having Mw *ca* 6.5). It is also more likely that the first-occurring earthquake is recorded in the sediments of subaquatic archives, as the slopes have to be recharged with sediment vulnerable to fail again. For the subsequent Verona earthquake from 1117 CE (52 years later), the slopes were likely not recharged yet, and no slope failure was triggered, thereby not leaving any traces from the earthquake in the sedimentary record of Lake Silvaplana. In Lake Ledro and Lake Iseo, which are located much closer to the epicentre, the Verona earthquake was detected (Simonneau *et al.*, 2013; Rapuc *et al.*, 2022).

The sediment cores from Lake Iseo (Rapuc *et al.*, 2022) have an event layer at 1120 to 1220 CE (interpreted to be caused by the Brescia earthquake in 1222 CE, Mw *ca* 6.0), an event layer at 1020 to 1125 CE (interpreted to be caused by the Verona earthquake in 1117 CE) and an event layer at 640 to 830 CE, lacking any documented earthquake. This oldest event layer coincides well with Event IV of Lake Silvaplana (480 to 670 CE, Fig. 16D), being the most prominent event deposit in both Lake Silvaplana (this study) and Lake Sils (Blass *et al.*, 2005; Nigg *et al.*, 2021), and also suggested for the sediment record of Lake Como (Fanetti *et al.*, 2008). In another sediment core from Lake Iseo (Lauterbach *et al.*, 2012), layers coinciding with Event IV from Lake Silvaplana, as well as the Verona earthquake in 1117 CE and Brescia earthquake in 1065 CE, were not identified, whereas the Brescia earthquake in 1222 CE is detected (Lauterbach *et al.*, 2012).

Churwalden was in 1295 CE the epicentre of an earthquake classified among the seven strongest of the last millennium in Switzerland (Mw *ca* 6.2; Schwarz-Zanetti *et al.*, 2004). Located within a short distance (*ca* 40 km; Fig. 1) of Lake Silvaplana, the Churwalden earthquake seems not to have triggered any large-scale slope failure. The estimated age of several thinner turbidites dated in our study correlate within the resolution of the age model to this historic earthquake. A reason for such a strong seismic event not triggering a megaturbidite could be that the Brescia earthquake 200 years before caused slope failure so that there was not enough time to recharge the slopes sufficiently to form the

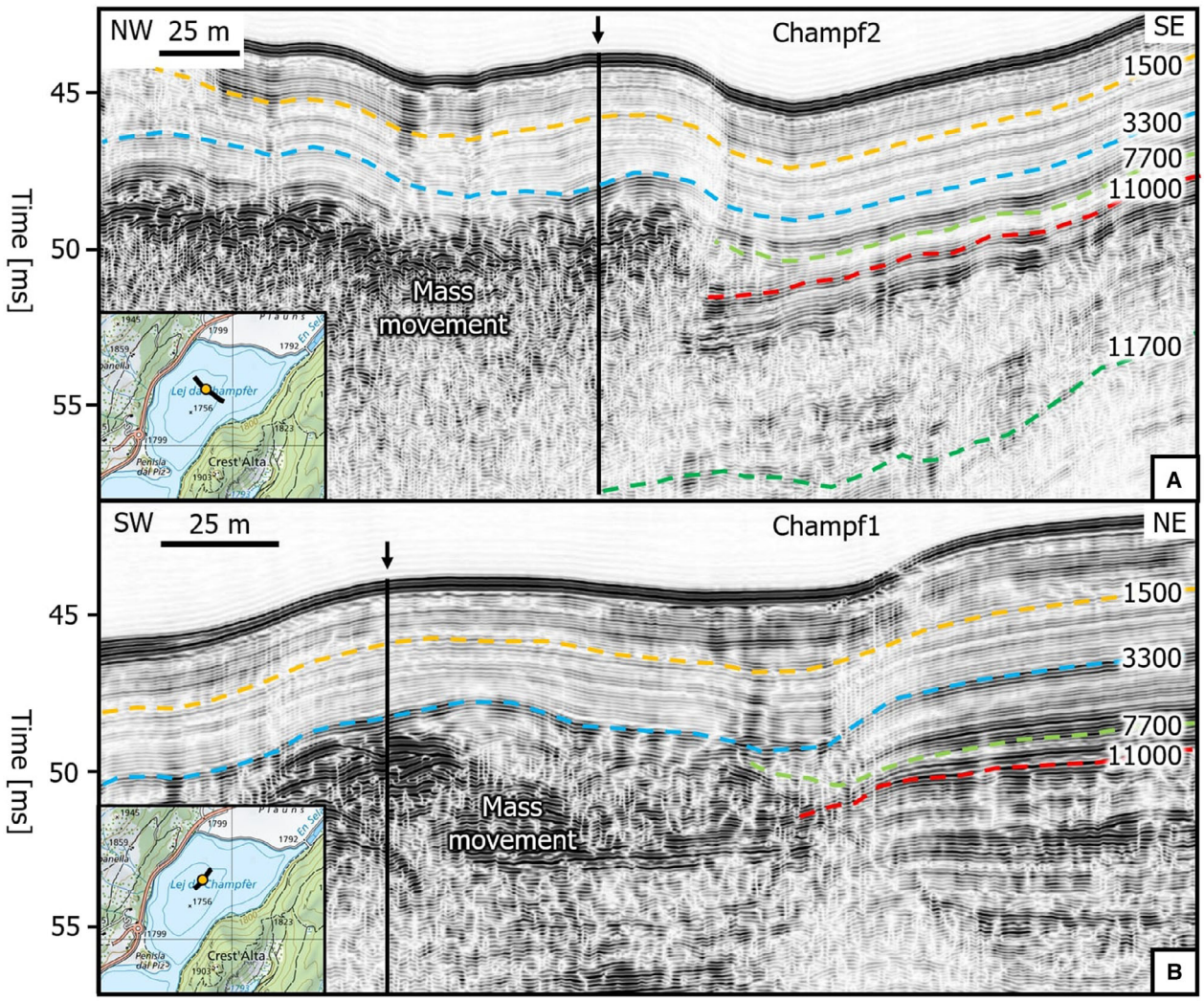

Fig. 17. Seismic stratigraphy of Lake Champfèr. (A) W-SE-oriented seismic profile. (B) SW-NE-oriented seismic profile. Seismic profiles from this study, with suggested ages of the seismic reflections based on age model of sediment core from Gobet *et al.* (2003). Indicated reflections represent age of Event IV in Lake Silvaplana (this study) at 1500 cal yr BP, change in sedimentation pattern in Lake Silvaplana (this study as well as Leemann & Niessen, 1994) at 3300 cal yr BP, base of SVA 12-2 (this study) at 7700 cal yr BP, the strong sedimentation change identified in Gobet *et al.* (2003) at 11 000 cal yr BP, and the base of sediment core of Gobet *et al.* (2003) at 11 700 cal yr BP.

load for large-volume sediment remobilization, similar as suggested for other Alpine lakes by Wilhelm *et al.* (2016). This would then imply that a certain amount of time is required for the recording of subsequent seismic events. Earthquake recurrence (time between seismic events), earthquake moment magnitude and distance to the epicentre all affect the sensitivity of seismically-triggered mass movements.

The megaturbidites documented in our study have not, or not to the same extent, been identified in previous studies of Lake Silvaplana (Leemann & Niessen, 1994; Gobet *et al.*, 2003; Blass *et al.*, 2007a,b; Trachsel *et al.*, 2008, 2010; Stewart *et al.*, 2011a,b). These previous studies focused on the identification of palaeofloods and summer temperature reconstructions, with the sediment cores located at the proximal Vallun Delta in shallower water depths to the south-east of Lake Silvaplana (Fig. 3B). A comparison of seismic cross-lines of Lake Silvaplana highlights that the megaturbidites are not deposited in these regions (Fig. 13) as they only appear further downslope (Fig. 13). Although not recording any megaturbidites, some of the mass flows have been cored in the previous studies (Event III and

IV in 90/2; potentially also in core 90/1; Leemann & Niessen, 1994). These mass flows may, however, consist of coherently remobilized deposits, or even sediments deformed *in situ*. While the mass flows have a clear signature in the seismic data shown in our study, they consisted of slightly deformed varves in the sediment core (LF2; Fig. 10C) so that it can be challenging to define mass flows when seismic data are lacking.

A strong temporal association between sediment-based events in Lake Silvaplana and neighbouring Lake Sils has been shown. The most prominent mass movement in Lake Silvaplana, Event IV, can be correlated to the thickest megaturbidite, a delta collapse and tsunami deposits of Lake Sils (Blass *et al.*, 2005; Nigg *et al.*, 2021). These lakes are characterized by similar stratigraphy and catchments, most likely reflecting similar processes active in the catchments and the lakes. Lake Champfèr is directly located to the north-east of Lake Silvaplana (Fig. 2). Whereas the two larger lakes of the Engadine Valley share similarities in both catchment and stratigraphy, Lake Champfèr is characterized by a thinner sediment package and smaller, non-glaciated catchment with no major tributary river input today. The seismic stratigraphy of Lake Champfèr shows that there was a very prominent mass movement at *ca* 7700 cal yr BP (age model from Gobet *et al.*, 2003), but there have not been any major slope failures since then (Fig. 17). The Late Holocene Events I to IV can neither be recognized in the seismic profiles of Lake Champfèr (Fig. 17) nor in the piston cores from the lake basin (Gobet *et al.*, 2003).

A comparison of the event stratigraphy of the different lake archives emphasizes that depositional environment and coring location are crucial for the completeness of earthquake records. Our study highlights the need for integrated interpretation for a successful characterization of palaeoseismic events using both seismic and sediment-core data. Furthermore, densely-spaced reflection seismic profiling is required to define appropriate coring locations for palaeoseismic event characterization.

Sensitivity for changes in sedimentation rate

The reconstructed changes in sedimentation rate in the last 7700 years of our study and that of Leemann & Niessen (1994) are in high agreement (Fig. 15). In this study, a change in sedimentation rate at *ca* 3300 cal yr BP has been identified, characterized by: (i) an upcore transition from lithofacies LF1b (dark and coarse-grained laminations) to lithofacies LF1a (bright and fine-grained laminations); (ii) an upcore change in sedimentation rate from <1 to 3 mm a^{-1}; (iii) a change in seismic amplitude strength from high-amplitude to moderate-amplitude; and (iv) an upcore decrease in magnetic susceptibility values within the flood layers. A similar transition at *ca* 3300 cal yr BP is also documented in the piston cores analysed by Leemann & Niessen (1994), characterized by: (i) sediment bulk accumulation increasing upcore, from <0.1 g cm^{-2} a to up to 0.3 g cm^{-2} a; (ii) an upcore decrease in organic carbon from >2% to <0.5%; (iii) an upcore decrease in median grain size from >15 to <8 μm; (iv) an upcore increase in flood frequency; and (v) an upcore change from lithofacies LF3 (dark laminations) to lithofacies LF2 (light-coloured varves). However, the change in sedimentation identified in our study is stronger and has a sharper transition compared with Leemann & Niessen (1994). In the sediment cores of Lake St. Moritz, a strong and slightly earlier transition is observed at *ca* 4000 cal yr BP (Gobet *et al.*, 2003) characterized by: (i) an upcore change in lithology from dark gyttja to bright gyttja; and (ii) a catchment-vegetation change from tree-dominated system to tree–shrub–herb balanced system.

Implications of the earthquake catalogue established in Lake Silvaplana

This study shows that at least four major earthquakes affected the Engadine Valley in the last 1400 years (Fig. 15). The bedrock ridges exposed on the lake floor indicate a correlation between ridge orientation and the tectonic Engadine Line (Figs 1 to 3). The bathymetric data of the bedrock ridge in the north-west of the lake show many slide scars, indicating frequent slope failure (Fig. 4B). The Engadine Line is further crossing the Isola Delta in Lake Sils, which collapsed and triggered a mass movement that coincides with Event IV (Fig. 2). The distribution of palaeoearthquakes listed in the Swiss earthquake inventory shows a concentration of palaeoepicentres along the Engadine Line (Fig. 1). This fault line might thus be a neotectonically active zone producing strong prehistorical earthquakes, as suggested by widespread gravity deformations in the Engadine Valley (Tibaldi & Pasquarè, 2008). However, the locally negative evidence of the earthquakes in Bormio (1999 CE) and in Churwalden (1295 CE) show the limitations of palaeoseismic records,

and imply challenges for sensitivity studies in slope stability and seismic activity.

Sedimentary event deposits identified in northern Italy coinciding with seismically-triggered event deposits of the Engadine Valley suggest the same seismic trigger in different geological archives (for example, lacustrine deposits, rock avalanches, archaeological sites) over larger distances (Fig. 16). The Swiss palaeoearthquake compilation thus has implications for seismic events located at larger distances in regions of neighbouring countries, such as northern Italy and western Austria. The catalogue is thus not only valid for the Engadine Valley, but should also be considered when assessing geohazards for regions of neighbouring countries.

CONCLUSIONS

The limnogeological investigations of Lake Silvaplana include a combination of high-resolution bathymetric maps, high-resolution reflection seismic profiles and a long sediment core. The stratigraphy, sedimentology and event chronology of the lake have been studied by detailed analysis of these datasets, and allow conclusions for the regional seismic activity.

The acoustic signal has an exceptionally high seismic penetration of up to 75 m in Lake Silvaplana. This high penetration allowed mapping of the acoustic basement, imaging of basin morphology and reconstruction of basin infill. Glaciers shaped the overdeepened palaeotopography by forming subaquatic moraines and sub-basins. Seismic and core data from the deepest basin highlight that the subsequent postglacial infill is dominated by finely laminated hemipelagic sediments intercalated with mass-movement deposits of coarser grain size.

Multiple simultaneously-triggered mass movements have been identified along ten seismostratigraphic horizons and indicate ten over-regional seismic events since glacial retreat. The uppermost four of these event deposits, consisting of megaturbidites and mass-flow wedges, have successfully been cored and radiocarbon dated. The authors interpret these ten event layers to be triggered by palaeoearthquakes in eastern Switzerland or northern Italy. Clusters of enhanced large-scale mass movements occur between 7800 and 11 300 cal yr BP, and in the last 1400 years. The deposits of Lake Silvaplana provide an ideal archive to study palaeoseismic activity of south-eastern Switzerland through the Holocene. The four seismic events are dated to 620 CE, 990 CE, 1640 CE and 1720 CE. These postulated palaeoearthquakes show strong age correlations with mass movements reported at about the same time in geological archives nearby. Two bedrock ridges following the Engadine Line further indicate the potential that the Engadine Line is a neotectonically active structure. This study concludes that the palaeoseismic record of Lake Silvaplana provides valuable insights into local seismic activity prior to the historically documented period, including larger earthquakes that likely triggered secondary events in Switzerland and its neighbouring countries.

ACKNOWLEDGEMENTS

We thank Helen Schönbächler and Reto Grischott for the technical support during fieldwork, and Alois Zwyssig for his help with sediment-core analysis. Irka Hajdas at the Laboratory of Ion Beam Physics Zurich of ETH Zürich and Sönke Szidat at the Laboratory for the Analysis of Radiocarbon with AMS (LARA) of the University of Bern are acknowledged for the radiocarbon dating. The acquisition of the bathymetric data was supported by the community of Silvaplana. We thank Associate Editor Rick Sarg, Marc De Batist, and the anonymous reviewers for their helpful comments and constructive feedback. Open access funding provided by Eidgenossische Technische Hochschule Zurich.

REFERENCES

Albini, P., **Bellani, A.** and **Stucchi, M.** (1988) Terremoti e frane nelle Alpi Centrali. In Atti del 7th Convegno annuale del GNDTS, Rome, Vol. **1**, 129–146.

Appleby, P.G. (2001) Chronostratigraphic techniques in recent sediments. In: *Tracking Environmental Change Using Lake Sediments Vol. 1: Basin Analysis, Coring, and Chronological Techniques* (Eds Last, W.M. and Smol, J.P.), Vol. **171**, p. 203. Springer, Dordrecht.

Badoux, A., **Andres, N.**, **Techel, F.** and **Hegg, C.** (2016) Natural hazard fatalities in Switzerland from 1946 to 2015. *Nat. Hazards Earth Syst. Sci.*, **16**, 2747–2768.

Baker, V.R. (2008) Paleoflood hydrology: origin, progress, prospects. *Geomorphology*, **101**, 1–13.

Beck, C., **Manalt, F.**, **Chapron, E.**, **van Rensbergen, P.** and **de Batist, M.** (1996) Enhanced seismicity in the early postglacial period: evidence from the post-Würm sediments of Lake Annecy, northwestern Alps. *J. Geodyn.*, **22**, 155–171.

Bellwald, B., **Hjelstuen, B.O.**, **Sejrup, H.P.** and **Haflidason, H.** (2016a) Postglacial mass movements and depositional environments in a high-latitude fjord system–Hardangerfjorden, Western Norway. *Mar. Geol.*, **379**, 157–175.

Bellwald, B., **Hjelstuen, B.O.**, **Sejrup, H.P.** and **Haflidason, H.** (2016b) Postglacial mass failures in the Inner Hardangerfjorden system, Western Norway. In: *Submarine Mass Movements and Their Consequences*, pp. 73–82. Springer, Cham.

Bellwald, B., **Hjelstuen, B.O.**, **Sejrup, H.P.**, **Stokowy, T.** and **Kuvås, J.** (2019a) Holocene mass movements in west and mid-Norwegian fjords and lakes. *Mar. Geol.*, **407**, 192–212.

Bellwald, B., **Urlaub, M.**, **Hjelstuen, B.O.**, **Sejrup, H.P.**, **Sørensen, M.B.**, **Forsberg, C.F.** and **Vanneste, M.** (2019b) NE Atlantic continental slope stability from a numerical modeling perspective. *Quat. Sci. Rev.*, **203**, 248–265.

van der Bilt, W.G., **Lane, C.S.** and **Bakke, J.** (2017) Ultra-distal Kamchatkan ash on Arctic Svalbard: towards hemispheric cryptotephra correlation. *Quat. Sci. Rev.*, **164**, 230–235.

Blaauw, M. and **Christen, J.A.** (2011) Flexible paleoclimate age-depth models using an autoregressive gamma process. *Bayesian Anal.*, **6**, 457–474.

Blass, A., **Anselmetti, F.S.**, **Grosjean, M.** and **Sturm, M.** (2005) The last 1300 years of environmental history recorded in the sediments of Lake Sils (Engadine, Switzerland). *Eclogae Geol. Helv.*, **98**, 319–332.

Blass, A., **Bigler, C.**, **Grosjean, M.** and **Sturm, M.** (2007a) Decadal-scale autumn temperature reconstruction back to AD 1580 inferred from the varved sediments of Lake Silvaplana (southeastern Swiss Alps). *Quatern. Res.*, **68**, 184–195.

Blass, A., **Grosjean, M.**, **Troxler, A.** and **Sturm, M.** (2007b) How stable are twentieth-century calibration models? A high-resolution summer temperature reconstruction for the eastern Swiss Alps back to AD 1580 derived from proglacial varved sediments. *Holocene*, **17**, 51–63.

Bogen, J. (1996) Erosion rates and sediment yields of glaciers. *Ann. Glaciol.*, **22**, 48–52.

Böhme, M., **Oppikofer, T.**, **Longva, O.**, **Jaboyedoff, M.**, **Hermanns, R.L.** and **Derron, M.H.** (2015) Analyses of past and present rock slope instabilities in a fjord valley: implications for hazard estimations. *Geomorphology*, **248**, 464–474.

Botzen, W.W., **Deschenes, O.** and **Sanders, M.** (2019) The economic impacts of natural disasters: a review of models and empirical studies. *Rev. Environ. Econ. Policy*, **13**, 167–188.

Bouma, A.H. (1987) Megaturbidite: an acceptable term? *Geo-Mar. Lett.*, **7**, 63–67.

Caviezel, G. (2007) *Hochwasser und ihre Bewältigung anhand des Beispiels Oberengadin 1750–1900*. Historisches Institut, Universität Bern, Bern.

Chapron, E., **Desmet, M.**, **De Putter, T.**, **Loutre, M.F.**, **Beck, C.** and **Deconinck, J.F.** (2002) Climatic variability in the northwestern Alps, France, as evidenced by 600 years of terrigenous sedimentation in Lake Le Bourget. *Holocene*, **12**, 177–185.

Chapron, E., **Arnaud, F.**, **Noël, H.**, **Revel, M.**, **Desmet, M.** and **Perdereau, L.** (2005) Rhone River flood deposits in Lake Le Bourget: a proxy for Holocene environmental changes in the NW Alps, France. *Boreas*, **34**, 404–416.

Chapron, E., **Simonneau, A.**, **Ledoux, G.**, **Arnaud, F.**, **Lajeunesse, P.** and **Albéric, P.** (2016) French Alpine Foreland Holocene paleoseismicity revealed by coeval mass wasting deposits in glacial lakes. In: *Submarine Mass Movements and their Consequences*, pp. 341–349. Springer, Cham.

Church, M. and **Slaymaker, O.** (1989) Disequilibrium of Holocene sediment yield in glaciated British Columbia. *Nature*, **337**, 452–454.

Clarke, J.E.H., **Marques, C.R.V.** and **Pratomo, D.** (2014) Imaging active mass-wasting and sediment flows on a fjord delta, Squamish, British Columbia. In: *Submarine Mass Movements and their Consequences*, pp. 249–260. Springer, Cham.

Cohen, A.S. (2003) *Paleolimnology: The History and Evolution of Lake Systems*. Oxford University Press, New York.

Czymzik, M., **Brauer, A.**, **Dulski, P.**, **Plessen, B.**, **Naumann, R.**, **von Grafenstein, U.** and **Scheffler, R.** (2013) Orbital and solar forcing of shifts in Mid-to Late Holocene flood intensity from varved sediments of pre-alpine Lake Ammersee (southern Germany). *Quat. Sci. Rev.*, **61**, 96–110.

De Gelder, G., **Doan, M.L.**, **Beck, C.**, **Carlut, J.**, **Seibert, C.**, **Feuillet, N.**, **Carter, G.**, **Pechlivanidou, S.** and **Gawthorpe, R.L.** (2022) Multi-scale and multi-parametric analysis of Late Quaternary event deposits within the active Corinth rift (Greece). *Sedimentology*, **69**, 1573–1598.

Dietrich, V. (1970) *Die Stratigraphie der Platta-Decke: Fazielle Zusammenhänge zwischen Oberpenninikum und Unterostalpin*. Geologisches Institut der Eidg. Technischen Hochschule und der Universität Zürich, Zürich.

ECOS-09. (2011) Earthquake Catalog of Switzerland 2009. Federal Earthquake Survey. http://www.seismo.ethz.ch/prod/catalog/index.

Erb, H., **Meyer, E.** and **Bruckner, A.** (1966) Römische Votivaltäre aus dem Engadin und neue Inschriften aus Chur. *Helvetia Antiqua, Festschrift Emil Vogt.*, **9**, 223–232.

Fabbri, S.C., **Buechi, M.W.**, **Horstmeyer, H.**, **Hilbe, M.**, **Hübscher, C.**, **Schmelzbach, C.**, **Weiss, B.** and **Anselmetti, F.S.** (2018) A subaquatic moraine complex in overdeepened Lake Thun (Switzerland) unravelling the deglaciation history of the Aare Glacier. *Quat. Sci. Rev.*, **187**, 62–79.

Fanetti, D., **Anselmetti, F.S.**, **Chapron, E.**, **Sturm, M.** and **Vezzoli, L.** (2008) Megaturbidite deposits in the Holocene basin fill of Lake Como (southern Alps, Italy). *Palaeogeogr. Palaeoclimatol. Palaeoecol.*, **259**, 323–340.

Gensler, G. and **Schüepp, M.** (1991) Witterungsklimatologie von Graubünden. In: *Beiträge zur Geographie Graubündens*, pp. 7–17. Egg, Zürich.

Giguet-Covex, C., **Arnaud, F.**, **Poulenard, J.**, **Disnar, J.R.**, **Delhon, C.**, **Francus, P.**, **David, F.**, **Enters, D.**, **Rey, P.-J.** and **Delannoy, J.J.** (2011) Changes in erosion patterns during the Holocene in a currently treeless subalpine catchment inferred from lake sediment geochemistry (Lake Anterne, 2063 m a.s.l., NW French Alps): the role of climate and human activities. *Holocene*, **21**, 651–665.

Gilli, A., **Anselmetti, F.S.**, **Glur, L.** and **Wirth, S.B.** (2013) Lake sediments as archives of recurrence rates and intensities of past flood events. In: *Dating Torrential Processes on Fans and Cones*, pp. 225–242. Springer, Dordrecht.

Girardclos, S., **Schmidt, O.T.**, **Sturm, M.**, **Ariztegui, D.**, **Pugin, A.** and **Anselmetti, F.S.** (2007) The 1996 AD delta collapse and large turbidite in Lake Brienz. *Mar. Geol.*, **241**(1–4), 137–154.

Glur, L., **Wirth, S.B.**, **Büntgen, U.**, **Gilli, A.**, **Haug, G.H.**, **Schär, C.**, **Beer, J.** and **Anselmetti, F.S.** (2013) Frequent floods in the European Alps coincide with cooler periods of the past 2500 years. *Sci. Rep.*, **3**, 1–5.

Glur, L., **Stalder, N.F.**, **Wirth, S.B.**, **Gilli, A.** and **Anselmetti, F.S.** (2015) Alpine lacustrine varved record reveals summer temperature as main control of glacier fluctuations over the past 2250 years. *Holocene*, **25**, 280–287.

Gobet, E., **Tinner, W.**, **Hochuli, P.A.**, **van Leeuwen, J.F.N.** and **Ammann, B.** (2003) Middle to Late Holocene vegetation history of the Upper Engadine (Swiss Alps): the role of man and fire. *Veg. Hist. Archaeobot.*, **12**, 143–163.

Guidoboni, E. and **Comastri, A.** (2005) *Catalogue of Earthquakes and Tsunamis in the Mediterranean Area from the 11th to the 15th Century*, p. 1037. Istituto nazionale di geofisica e vulcanologia, Rome, Italy.

Guidoboni, E., **Comastri, A.** and **Boschi, E.** (2005) The "exceptional" earthquake of 3 January 1117 in the Verona area (northern Italy): A critical time review and detection of two lost earthquakes (lower Germany and Tuscany). *J. Geophys. Res. Solid Earth*, **110**(B12), 1–20.

Guidoboni, E., **Ferrari, G.**, **Mariotti, D.**, **Comastri, A.**, **Tarabusi, G.** and **Valensise, G.** (2007) CFTI4Med, Catalogue of Strong Earthquakes in Italy (461 B.C.-1997) and Mediterranean Area (760 B.C.-1500). *INGV-SGA*. Available at: http://storing.ingv.it/cfti4med/.

Hermanns, R.L., **Schleier, M.**, **Böhme, M.**, **Blikra, L.H.**, **Gosse, J.**, **Ivy-Ochs, S.** and **Hilger, P.** (2017) Rock-avalanche activity in W and S Norway peaks after the retreat of the Scandinavian Ice Sheet. In: *Workshop on World Landslide Forum*, pp. 331–338. Springer, Cham.

Hilbe, M. and **Anselmetti, F.S.** (2015) Mass movement-induced tsunami hazard on perialpine Lake Lucerne (Switzerland): scenarios and numerical experiments. *Pure Appl. Geophys.*, **172**, 545–568.

Hilbe, M., **Anselmetti, F.S.**, **Eilertsen, R.S.**, **Hansen, L.** and **Wildi, W.** (2011) Subaqueous morphology of Lake Lucerne (Central Switzerland): implications for mass movements and glacial history. *Swiss J. Geosci.*, **104**, 425–443.

Huggel, C., **Haeberli, W.**, **Kääb, A.**, **Bieri, D.** and **Richardson, S.** (2004) An assessment procedure for glacial hazards in the Swiss Alps. *Can. Geotech. J.*, **41**, 1068–1083.

Huss, M., **Bauder, A.**, **Werder, M.**, **Funk, M.** and **Hock, R.** (2007) Glacier-dammed lake outburst events of Gornersee, Switzerland. *J. Glaciol.*, **53**, 189–200.

Hydrodaten.admin.ch Federal Office for the Environment FOEN – Hydrological data and forecasts. https://www.hydrodaten.admin.ch/en/2072.html.

Ilyashuk, B., **Gobet, E.**, **Heiri, O.**, **Lotter, A.F.**, **van Leeuwen, J.F.**, **van der Knaap, W.O.**, **Ilyashuk, E.**, **Oberli, F.** and **Ammann, B.** (2009) Lateglacial environmental and climatic changes at the Maloja Pass, Central Swiss Alps, as recorded by chironomids and pollen. *Quat. Sci. Rev.*, **28**, 1340–1353.

Ivy-Ochs, S., **Kerschner, H.**, **Reuther, A.**, **Preusser, F.**, **Heine, K.**, **Maisch, M.**, **Kubik, P.W.** and **Schlüchter, C.** (2008) Chronology of the last glacial cycle in the European Alps. *J. Quat. Sci.*, **23**, 559–573.

Ivy-Ochs, S., **Martin, S.**, **Campedel, P.**, **Hippe, K.**, **Alfimov, V.**, **Vockenhuber, C.**, **Andreotti, E.**, **Carugati, G.**, **Pasqual, D.**, **Rigo, M.** and **Viganò, A.** (2017) Geomorphology and age of the Marocche di Dro rock avalanches (Trentino, Italy). *Quat. Sci. Rev.*, **169**, 188–205.

Knapp, S., **Gilli, A.**, **Anselmetti, F.S.**, **Krautblatter, M.** and **Hajdas, I.** (2018) Multistage rock-slope failures revealed in lake sediments in a seismically active Alpine region (Lake Oeschinen, Switzerland). *J. Geophys. Res. Earth*, **123**, 658–677.

Kremer, K., **Marillier, F.**, **Hilbe, M.**, **Simpson, G.**, **Dupuy, D.**, **Yrro, B.J.**, **Rachoud-Schneider, A.**, **Corboud, P.**, **Bellwald, B.**, **Wildi, W.** and **Girardclos, S.** (2014) Lake dwellers occupation gap in Lake Geneva (France–Switzerland) possibly explained by an earthquake–mass movement–tsunami event during Early Bronze Age. *Earth Planet. Sci. Lett.*, **385**, 28–39.

Kremer, K., **Wirth, S.B.**, **Reusch, A.**, **Fäh, D.**, **Bellwald, B.**, **Anselmetti, F.S.**, **Girardclos, S.** and **Strasser, M.** (2017) Lake-sediment based paleoseismology: Limitations and perspectives from the Swiss Alps. *Quat. Sci. Rev.*, **168**, 1–18.

Kremer, K., **Gassner-Stamm, G.**, **Grolimund, R.**, **Wirth, S.B.**, **Strasser, M.** and **Fäh, D.** (2020a) A database of potential paleoseismic evidence in Switzerland. *J. Seismol.*, **24**, 247–262.

Kremer, K., **Anselmetti, F.S.**, **Evers, F.M.**, **Goff, J.** and **Nigg, V.** (2021) Freshwater (paleo) tsunamis—a review. *Earth-Sci. Rev.*, **212**, 103447.

Kulbe, T., **Anselmetti, F.**, **Cantonati, M.** and **Sturm, M.** (2005) Environmental history of Lago di Tovel, Trento, Italy, revealed by sediment cores and 3.5 kHz seismic mapping. *J. Paleolimnol.*, **34**, 325–337.

Lauterbach, S., **Chapron, E.**, **Brauer, A.**, **Hüls, M.**, **Gilli, A.**, **Arnaud, F.**, **Andrea, P.**, **Jérôme, N.**, **Marc, D.**, **Ulrich, G.** and **Participants, D.** (2012) A sedimentary record of Holocene surface runoff events and earthquake activity from Lake Iseo (Southern Alps, Italy). *Holocene*, **22**, 749–760.

Lee, H.J. (2009) Timing of occurrence of large submarine landslides on the Atlantic Ocean margin. *Mar. Geol.*, **264**, 53–64.

Leemann, A. and **Niessen, F.** (1994) Holocene glacial activity and climatic variations in the Swiss Alps: reconstructing a continuous record from proglacial lake sediments. *Holocene*, **4**, 259–268.

L'Heureux, J.S., **Glimsdal, S.**, **Longva, O.**, **Hansen, L.** and **Harbitz, C.B.** (2011) The 1888 shoreline landslide and tsunami in Trondheimsfjorden, central Norway. *Mar. Geophys. Res.*, **32**, 313–329.

LIMNEX (1994) *Gewässerzustand und Gewässerschutz massnahmen im Oberengadin*. Bericht zuhanden des Amtes für Umweltschutz, Kanton Graubuenden.

LIMNEX (2004) *Gewässerzustand und Gewässerschutz massnahmen im Oberengadin*. Bericht zuhanden des Amtes für Umweltschutz, Kanton Graubünden.

LIMNEX (2011) *Gewässerzustand und Gewässerschutz massnahmen im Oberengadin*. Bericht zuhanden des Amtes für Umweltschutz, Kanton Graubünden.

Livio, F.A., **Ferrario, M.F.**, **Martinelli, E.**, **Talamo, S.**, **Michetti, A.M.** and **Cercatillo, S.** (2023) The footprint of an ancient forgotten earthquake: a VI Cent. AD event in the European Western Southern Alps. *Nat. Hazards Earth Syst. Sci. Discuss.*, **2023**, 1–23.

Maisch, M. (1992) *Die Gletscher des Graubündens*. Habil Schrift Geogr. Inst. Univ. Zürich, Teil A und B, Zürich.

Moernaut, J., **De Batist, M.**, **Charlet, F.**, **Heirman, K.**, **Chapron, E.**, **Pino, M.**, **Brümmer, R.** and **Urrutia, R.** (2007) Giant earthquakes in South-Central Chile revealed by Holocene mass-wasting events in Lake Puyehue. *Sediment. Geol.*, **195**, 239–256.

Monecke, K., **Anselmetti, F.S.**, **Becker, A.**, **Schnellmann, M.**, **Sturm, M.** and **Giardini, D.** (2006) Earthquake-induced deformation structures in lake deposits: a late Pleistocene to Holocene paleoseismic record for Central Switzerland. *Eclogae Geol. Helv.*, **99**, 343–362.

Mulder, T. and **Cochonat, P.** (1996) Classification of offshore mass movements. *J. Sediment. Res.*, **66**, 43–57.

NFP. (1998) Glaziologische Karte Julier-Bernina (Oberengadin). Nationales Forschungsprogramm "Klimaänderungen und Naturkatastrophen" (NFP 31). 1. Auflage. 36 pp.

Nigg, V., **Wohlwend, S.**, **Hilbe, M.**, **Bellwald, B.**, **Fabbri, S.C.**, **de Souza, G.F.**, **Donau, F.**, **Grischott, R.**, **Strasser, M.** and **Anselmetti, F.S.** (2021) A tsunamigenic delta collapse and its associated tsunami deposits in and around Lake Sils, Switzerland. *Nat. Hazards*, **107**, 1069–1103.

Nussbaumer, S.U., **Steinhilber, F.**, **Trachsel, M.**, **Breitenmoser, P.**, **Beer, J.**, **Blass, A.**, **Grosjean, M.**, **Hafner, A.**, **Holzhauser, H.**, **Wanner, H.** and **Zumbühl, H.J.** (2011) Alpine climate during the Holocene: a comparison between records of glaciers, lake sediments and solar activity. *J. Quat. Sci.*, **26**, 703–713.

Ohlendorf, C., **Niessen, F.** and **Weissert, H.** (1997) Glacial varve thickness and 127 years of instrumental climate data: a comparison. In: *Climatic Change at High Elevation Sites*, pp. 159–179. Springer, Dordrecht.

Oswald, P., **Strasser, M.**, **Hammerl, C.** and **Moernaut, J.** (2021) Seismic control of large prehistoric rockslides in the Eastern Alps. *Nat. Commun.*, **12**, 1059.

Peters, T. (2005) Geologischer Atlas der Schweiz 1:25000, 1257 St. Moritz, Atlasblatt 118, Erläuterungen. Bundesamt für Wasser und Geologie.

Praet, N., **Moernaut, J.**, **van Daele, M.**, **Boes, E.**, **Haeussler, P.J.**, **Strupler, M.**, **Schmidt, S.**, **Loso, M.G.** and **De Batist, M.** (2017) Paleoseismic potential of sublacustrine landslide records in a high-seismicity setting (south-central Alaska). *Mar. Geol.*, **384**, 103–119.

Ramsey, C.B. (2009) Bayesian analysis of radiocarbon dates. *Radiocarbon*, **51**, 337–360.

Rapuc, W., **Arnaud, F.**, **Sabatier, P.**, **Anselmetti, F.S.**, **Piccin, A.**, **Peruzza, L.**, **Bastien, A.**, **Augustin, L.**, **Régnier, E.**, **Gaillardet, J.** and **von Grafenstein, U.** (2022) Instant sedimentation in a deep Alpine lake (Iseo, Italy) controlled by climate, human and geodynamic forcing. *Sedimentology*, **69**(4), 1816–1840.

Reimer, P., **Bard, E.**, **Bayliss, A.**, **Beck, J.**, **Blackwell, P.**, **Ramsey, C.**, **Buck, C.E.**, **Cheng, H.**, **Edwards, R.L.**, **Friedrich, M.**, **Grootes, P.M.**, **Guilderson, T.P.**, **Haflidason, H.**, **Hajdas, I.**, **Hatté, C.**, **Heaton, T.J.**, **Hoffmann, D.L.**, **Hogg, A.G.**, **Hughen, K.A.**, **Kaiser, K.F.**, **Kromer, B.**, **Manning, S.W.**, **Niu, M.**, **Reimer, R.W.**, **Richards, D.A.**, **Scott, E.M.**, **Southon, J.R.**, **Staff, R.** and **Van der Plicht, J.** (2013) IntCal13 and Marine13 radiocarbon age calibration curves 0–50,000 years cal BP. *Radiocarbon*, **55**, 1869–1887.

Sammartini, M., **Moernaut, J.**, **Kopf, A.**, **Stegmann, S.**, **Fabbri, S.C.**, **Anselmetti, F.S.** and **Strasser, M.** (2021) Propagation of frontally confined subaqueous landslides: insights from combining geophysical, sedimentological, and geotechnical analysis. *Sediment. Geol.*, **416**, 105877.

Sanders, D., **Wallner, M.** and **Pomella, H.** (2021) Medieval age determined for the hitherto undescribed/undated rock avalanche of Münster (Inn valley, Eastern Alps). *Geomorphology*, **389**, 107802.

Schlüchter, C. (1987) Talgenese im Quartär: Eine Standortbestimmung. *Geographica Helvetica*, **42**, 109–115.

Schlüchter, C., **Bonani, G.**, **Donau, F.**, **Grischott, R.**, **Nicolussi, K.**, **Pfenninger, A.**, **Schlüchter, B.**, **Seifert, M.**, **Vattioni, S.** and **Hajdas, I.** (2018) Rätselhafte Unterwasserbäume in den Oberengadiner Seen. *Jahresbericht der Naturforschenden Gesellschaft Graubünden*, **120**, 41–49.

Schmid, S.M. and **Froitzheim, N.** (1993) Oblique slip and block rotation along the Engadine line. *Eclogae Geol. Helv.*, **86**, 569–593.

Schneider, J., **Flemings, P.B.**, **Dugan, B.**, **Long, H.** and **Germaine, J.T.** (2009) Overpressure and consolidation near the seafloor of Brazos-Trinity Basin IV, northwest deepwater Gulf of Mexico. *J. Geophys. Res. Solid Earth*, **114**(B5). https://doi.org/10.1029/2008JB005922

Schnellmann, M., **Anselmetti, F.S.**, **Giardini, D.**, **McKenzie, J.A.** and **Ward, S.N.** (2002) Prehistoric earthquake history revealed by lacustrine slump deposits. *Geology*, **30**, 1131–1134.

Schnellmann, M., **Anselmetti, F.S.**, **Giardini, D.** and **McKenzie, J.A.** (2005) Mass movement-induced fold-and-thrust belt structures in unconsolidated sediments in Lake Lucerne (Switzerland). *Sedimentology*, **52**, 271–289.

Schnellmann, M., **Anselmetti, F.S.**, **Giardini, D.** and **Mckenzie, J.A.** (2006) 15,000 years of mass-movement history in Lake Lucerne: implications for seismic and tsunami hazards. *Eclogae Geol. Helv.*, **99**, 409–428.

Schwarz-Zanetti, G., **Deichmann, N.**, **Fäh, D.**, **Masciadri, V.** and **Goll, J.** (2004) The earthquake in Churwalden (CH) of September 3, 1295. *Eclogae Geol. Helv.*, **97**, 255–264.

Simonneau, A., **Chapron, E.**, **Vannière, B.**, **Wirth, S.B.**, **Gilli, A.**, **Di Giovanni, C.**, **Anselmetti, F.S.**, **Desmet, M.** and **Magny, M.** (2013) Mass-movement and flood-induced deposits in Lake Ledro, southern Alps, Italy: implications for Holocene palaeohydrology and natural hazards. *Clim. Past*, **9**, 825–840.

Slootman, A. and **Cartigny, M.J.** (2020) Cyclic steps: review and aggradation-based classification. *Earth-Sci. Rev.*, **201**, 102949.

Spillmann, P. and **Büchi, H.J.** (1993) The Pre-alpine basement of the lower austro-alpine nappes in the bernina massif (Grisons, Switzerland; Valtellina, Italy). In: *Pre-Mesozoic Geology in the Alps*, pp. 457–467. Springer, Berlin, Heidelberg.

Stewart, M.M., **Grosjean, M.**, **Kuglitsch, F.G.**, **Nussbaumer, S.U.** and **von Gunten, L.** (2011a) Reconstructions of late Holocene paleofloods and glacier length changes in the Upper Engadine, Switzerland (ca. 1450 BC–AD 420). *Palaeogeogr. Palaeoclimatol. Palaeoecol.*, **311**, 215–223.

Stewart, M.M., **Larocque-Tobler, I.** and **Grosjean, M.** (2011b) Quantitative inter-annual and decadal June–July–August temperature variability ca. 570 BC to AD 120 (Iron Age–Roman Period) reconstructed from the varved sediments of Lake Silvaplana, Switzerland. *J. Quat. Sci.*, **26**, 491–501.

Støren, E.N., **Dahl, S.O.**, **Nesje, A.** and **Paasche, Ø.** (2010) Identifying the sedimentary imprint of high-frequency Holocene river floods in lake sediments: development and application of a new method. *Quat. Sci. Rev.*, **29**, 3021–3033.

Støren, E.W., **Paasche, Ø.**, **Hirt, A.M.** and **Kumari, M.** (2016) Magnetic and geochemical signatures of flood layers in a lake system. *Geochem. Geophys. Geosyst.*, **17**, 4236–4253.

Strasser, M. and **Anselmetti, F.** (2008) Mass-movement event stratigraphy in Lake Zurich; A record of varying seismic and environmental impacts. *Beiträge zur Geologie der Schweiz, Geotechnische Serie*, **95**, 23–41.

Strasser, M., **Anselmetti, F.S.**, **Fäh, D.**, **Giardini, D.** and **Schnellmann, M.** (2006) Magnitudes and source areas of large prehistoric northern Alpine earthquakes revealed by slope failures in lakes. *Geology*, **34**, 1005–1008.

Strasser, M., **Monecke, K.**, **Schnellmann, M.** and **Anselmetti, F.S.** (2013) Lake sediments as natural seismographs: a compiled record of Late Quaternary earthquakes in Central Switzerland and its implication for Alpine deformation. *Sedimentology*, **60**, 319–341.

Strupler, M., **Hilbe, M.**, **Kremer, K.**, **Danciu, L.**, **Anselmetti, F.S.**, **Strasser, M.** and **Wiemer, S.** (2018) Subaqueous

landslide-triggered tsunami hazard for Lake Zurich, Switzerland. *Swiss J. Geosci.*, **111**, 353–371.

Sturm, M. and **Matter, A.** (1978) Turbidites and varves in Lake Brienz (Switzerland): deposition of clastic detritus by density currents. In: *Modern and Ancient Lake Sediments* (Eds Matter, A. and Tucker, M.E.), pp. 147–168. Wiley, Hoboken.

Sturm, M., **Siegenthaler, C.** and **Pickrill, R.A.** (1995) Turbidites and "homogenites"–a conceptual model of flood and slide deposits. In: *Publication of IAS-16th Regional Meeting Sedimentology, Paris*, Vol. **22**, p. 140.

Swierczynski, T., **Lauterbach, S.**, **Dulski, P.**, **Delgado, J.**, **Merz, B.** and **Brauer, A.** (2013) Mid-to late Holocene flood frequency changes in the northeastern Alps as recorded in varved sediments of Lake Mondsee (Upper Austria). *Quat. Sci. Rev.*, **80**, 78–90.

Szidat, S., **Salazar, G.A.**, **Vogel, E.**, **Battaglia, M.**, **Wacker, L.**, **Synal, H.A.** and **Türler, A.** (2014) 14C analysis and sample preparation at the new Bern Laboratory for the Analysis of Radiocarbon with AMS (LARA). *Radiocarbon*, **56**, 561–566.

Tibaldi, A. and **Pasquarè, F.A.** (2008) Quaternary deformations along the 'Engadine–Gruf tectonic system', Swiss–Italian Alps. *J. Quat. Sci.*, **23**, 475–487.

Trachsel, M., **Eggenberger, U.**, **Grosjean, M.**, **Blass, A.** and **Sturm, M.** (2008) Mineralogy-based quantitative precipitation and temperature reconstructions from annually laminated lake sediments (Swiss Alps) since AD 1580. *Geophys. Res. Lett.*, **35**. https://doi.org/10.1029/2008GL034121

Trachsel, M., **Grosjean, M.**, **Larocque-Tobler, I.**, **Schwikowski, M.**, **Blass, A.** and **Sturm, M.** (2010) Quantitative summer temperature reconstruction derived from a combined biogenic Si and chironomid record from varved sediments of Lake Silvaplana (south-eastern Swiss Alps) back to AD 1177. *Quat. Sci. Rev.*, **29**, 2719–2730.

Vandekerkhove, E., **Bertrand, S.**, **Torrejón, F.**, **Kylander, M.E.**, **Reid, B.** and **Saunders, K.M.** (2021) Signature of modern glacial lake outburst floods in fjord sediments (Baker River, southern Chile). *Sedimentology*, **68**, 2798–2819.

Vasskog, K., **Nesje, A.**, **Støren, E.N.**, **Waldmann, N.**, **Chapron, E.** and **Ariztegui, D.** (2011) A Holocene record of snow-avalanche and flood activity reconstructed from a lacustrine sedimentary sequence in Oldevatnet, western Norway. *Holocene*, **21**, 597–614.

Wilhelm, B., **Nomade, J.**, **Crouzet, C.**, **Litty, C.**, **Sabatier, P.**, **Belle, S.**, **Rolland, Y.**, **Revel, M.**, **Courboulex, F.**, **Arnaud, F.** and **Anselmetti, F.S.** (2016) Quantified sensitivity of small lake sediments to record historic earthquakes: implications for paleoseismology. *J. Geophys. Res. Earth*, **121**, 2–16.

Wirth, S.B., **Glur, L.**, **Gilli, A.** and **Anselmetti, F.S.** (2013) Holocene flood frequency across the Central Alps–solar forcing and evidence for variations in North Atlantic atmospheric circulation. *Quat. Sci. Rev.*, **80**, 112–128.

www.engadin.ch/en. Report Facts and Figures of Engadin St. Moritz Tourismus AG, Seasons 2017 and 2018. 20 pp.

Zoller, H. and **Brombacher, C.** (1984) Das Pollenprofil Chavlus bei St.Moritz—ein Beitrag zur Wald- und Landwirtschaftsgeschichte im Oberengadin. *Dissertationes Botanicae*, **72**, 377–398.

Manuscript received 7 December 2021; revision accepted 17 July 2023

Supporting Information

Additional information may be found in the online version of this article:

Data S1 Figure S1. Composite section consisting of short core (SC; SVA 12-1) and two long cores (SVA 12-2 and SVA 12-3). Black line indicates which segments were used for the final composite section.

Table S1. Depths for age model and event catalogue.